Atmospheric
Chemistry
and Physics
Discussions

1 **US surface ozone trends and extremes from 1980-2014: Quantifying the roles of**
2 **rising Asian emissions, domestic controls, wildfires, and climate**
3
4 Meiyun Lin[1,2*], Larry W. Horowitz[2], Richard Payton[3], Arlene M. Fiore[4], Gail Tonnesen[3]
5
6 [1]*Atmospheric and Oceanic Sciences, Princeton University, Princeton,* NJ *08540, USA*
7 [2]*NOAA Geophysical Fluid Dynamics Laboratory, Princeton, NJ 08540, USA*
8 [3]*U.S. Environmental Protection Agency, Region 8, Denver, CO 80202, USA*
9 [4]*Lamont-Doherty Earth-Observatory and Department of Earth and Environmental*
10 *Sciences, Columbia University, Palisades, NY 10964, USA*
11
12 ***Corresponding Author:**
13 Meiyun Lin (Email: Meiyun.Lin@noaa.gov; Phone: 1-609 452-6551)
14

15 **Abstract.** Surface ozone (O_3) responds to varying global-to-regional precursor emissions,
16 climate, and extreme weather, with implications for designing effective air quality control
17 policies. We examine these conjoined processes with observations and global
18 chemistry-climate model (GFDL-AM3) hindcasts over 1980-2014. The model captures
19 the salient features of observed trends in daily maximum 8-hour average O_3; (1) increases
20 over East Asia (up to 2 ppb yr^{-1}), (2) springtime increases at western US (WUS) rural
21 sites (0.2-0.5 ppb yr^{-1}) with a 'baseline' sampling approach, (3) summertime decreases,
22 largest at the 95th percentile, and wintertime increases in the 50th to 5th percentiles over
23 the eastern US (EUS). Asian NO$_x$ emissions tripled since 1990, contributing as much as
24 65% to modeled springtime background O_3 increases (0.3-0.5 ppb yr^{-1}) over the WUS,
25 outpacing O_3 decreases attained via US domestic emission controls. Methane increases
26 over this period raise WUS background O_3 by 15%. During summer, increasing Asian
27 emissions approximately offset the effects of US emission reductions, leading to weak or
28 insignificant observed O_3 trends at WUS rural sites. While wildfire emissions can
29 enhance summertime monthly mean O_3 at individual sites by 2-8 ppb, high temperatures
30 and the associated buildup of O_3 produced from regional anthropogenic emissions
31 contribute most to elevating observed summertime O_3 throughout the USA. Rising Asian
32 emissions and global methane under the RCP8.5 scenario increase mean springtime O_3
33 above the WUS by ~10 ppb from 2010 to 2030. Historical EUS O_3 decreases, driven by
34 regional emission controls, were most pronounced in the Southeast with an earlier onset
35 of biogenic isoprene emissions and NO$_x$-sensitive O_3 production. Regional NO$_x$
36 reductions also alleviated the O_3 buildup during the recent heat waves of 2011 and 2012
37 relative to earlier heat waves (e.g., 1988; 1999). Without emission controls, the 95th
38 percentile summertime O_3 in the EUS would have increased by 0.2-0.4 ppb yr^{-1} over
39 1988-2014 due to more frequent hot extremes and rising biogenic isoprene emissions.
40
41

Atmospheric
Chemistry
and Physics
Discussions

Open Access

1. Introduction

Decreases in summertime O_3 were observed in parts of California and throughout the EUS (e.g., *Cooper et al., 2012; Simon et al., 2015*), following regional NO_x controls after the lowering of the US National Ambient Air Quality Standard (NAAQS) for O_3 in 1997 to 84 ppb. On the basis of health evidence, the NAAQS level for O_3 has been further lowered to 75 ppb in 2008 and to 70 ppb in 2015 (*Federal Register, 2015*). There are concerns that increases in Asian anthropogenic emissions (*Jacob et al., 1999; Lin et al., 2015b*), more frequent large wildfires in summer (e.g., *Jaffe, 2011*; *Yang et al.*, 2015; *Abatzoglou et al., 2016*), and late spring deep stratospheric O_3 intrusions (*Lin et al., 2012a*; *Langford et al., 2014; Lin et al., 2015a*) may pose challenges in attaining more stringent O_3 standards at high-elevation WUS regions. A warming climate would also offset some of air quality improvements gained from regional emission controls (see review by *Fiore et al., 2015*). Quantitative understanding on sources of O_3 variability on daily to multi-decadal time scales can provide valuable information to air quality control managers as they develop O_3 abatement strategies under the NAAQS. Here we systemically investigate the response of US surface O_3 means and extremes to changes in Asian and North American anthropogenic emissions, global methane, regional heat waves and wildfires over the course of 35 years from 1980 to 2014, using a suite of observations and chemistry-climate model (GFDL-AM3) hindcasts (*Lin et al., 2014; 2015a; 2015b*).

Rapid economic growth has led to a tripling of O_3 precursor emissions from Asia in the past 25 years (e.g., *Granier et al., 2011; Hillboll et al., 2013*). Observed 1-hour O_3 mixing ratios can frequently reach 200-400 ppb during regional pollution episodes in eastern China (*Wang T. et al.,* 2006; *Li et al., 2016*), with a seasonal peak in the late spring to early summer (*Wang Y. et al., 2008; Lin et al., 2009*). A synthesis of available observations from the mid-1990s to the 2000s indicates increases of 1-2 ppb yr^{-1} in spring to summer O_3 in China (*Ding et al., 2008; Ma et al., 2015; Sun et al., 2015*). Long-range transport of Asian pollution plumes towards western North America has been identified by aircraft and satellite measurements and in chemical transport models (e.g., *Jaffe et al., 1999; Zhang et al.,* 2008; *Fiore et al., 2009; Lin et al., 2012b; Huang et al., 2013; Verstraeten et al., 2015*). Systematic comparison of observed and modeled long-term O_3 trends over Asia is lacking in the published literature, but is needed to establish confidence in models used to assess the global impacts of rising Asian emissions.

Import of Asian pollution enhances mean WUS surface O_3 in spring by 5 ppb, and occasionally contributes 8-15 ppb during springtime pollution episodes observed at rural sites (*Lin et al., 2012b*). Stratospheric intrusions can episodically increase daily 8-hour average surface O_3 by 20-40 ppb, contributing to the highest observed O_3 events at high-elevation WUS sites (*Lin et al., 2012a; Lin et al., 2015*), in addition to pollution transport from California (e.g., *Langford et al.*, 2010). In the densely populated EUS, both changes in regional anthropogenic emissions and air pollution meteorology have the greatest impacts on summer surface O_3 during pollution episodes (*e.g., Jacob and Winner 2009; Rieder et al., 2015; Porter et al., 2015; Pusede et al., 2015*). Discerning directly

Atmospheric
Chemistry
and Physics
Discussions

1   the effect of climate change on air quality from long-term observation records of O_3
2   would be ideal, but concurrent trends in precursor emissions impede such an effort. It is
3   difficult to separate the impacts of changes in global-to-regional precursor emissions and
4   different meteorological factors on O_3 at given locations without the benefit of multiple
5   sensitivity experiments afforded by models.

6   On the other hand, process-oriented assessments of the models are needed to build
7   confidence in their utility for assessing pollution control strategies, estimating
8   tropospheric O_3 radiative forcing and projecting pollution extremes under future climate
9   scenarios (e.g., *Monks et al., 2015*). A number of studies show that global models capture
10   observed decreases in summertime O_3 over the EUS during 1990-2010, but have
11   difficulty simulating O_3 increases measured at remote high-altitude sites that are believed
12   to represent hemispheric-scale conditions with little influence from fresh local pollution
13   (hereafter referred to as "baseline") (e.g., *Lamarque et al., 2010*; *Koumoutsaris and Bey,*
14   *2012; Parrish et al., 2014; Brown-Steiner and Hess 2014; Strode et al., 2015*). Recently,
15   *Lin et al.* (2015b) examined the representativeness of O_3 trends derived from sparse
16   measurements in the free troposphere over the WUS, originally reported by *Cooper et al.*
17   (2010) and used in previous model evaluations. They found that discrepancies between
18   observed and simulated O_3 trends reflect measurement sampling biases. Here we seek
19   additional insights into the causes of the model-observation disagreement at the WUS
20   rural sites with continuous, high-frequency measurements. Notably, we reconcile
21   observed and simulated O_3 trends at these sites with a baseline sampling approach.

22   Our goal in this paper is twofold: first, to systematically evaluate how well our
23   GFDL-AM3 BASE simulation represents trends and variability of surface O_3 observed at
24   rural sites across the US; second, to examine changes in US surface O_3 means and
25   extremes in a suite of multi-decadal hindcast simulations designed to isolate the response
26   of O_3 to increases in Asian anthropogenic emissions, North American emission controls,
27   rising global methane, wildfires, and interannual variability in meteorology. We examine
28   trends across the entire probability distribution of O_3 concentration, which is crucial to
29   assessing the ability of models to simulate the surface O_3 response under different
30   temperature and chemical regimes depending on seasons, geographical location, and
31   regional transport patterns. Specifically, we evaluate the trends separately for the 5th, 50th
32   and 95th percentiles of the O_3 concentration distribution in spring (March-April-May;
33   MAM), summer (June-July-August; JJA), and winter (December-January-February;
34   DJF).

35   Section 2 briefly describes the observational records, model experiments, and
36   analysis approach. As a first step towards assessing our understanding of the impacts of
37   rising Asian emissions, we briefly review Asian O_3 trends from observations in recent
38   publications and evaluate modeled trends (Sect. 3). We then focus our analysis on the US,
39   using both observations and models to assess the response of US surface O_3 to changes in
40   background O_3, regional anthropogenic emissions and meteorology (Sect. 4). In Section 5,
41   we further separate the influence of background on WUS O_3 into components driven by

Atmospheric
Chemistry
and Physics
Discussions

1   rising Asian anthropogenic emissions, global methane, and wildfires. We quantify the
2   contribution of these factors to surface O_3 in both rural areas such as national parks (Sect.
3   5.1 to 5.3) and in densely populated regions such as the Denver Metropolitan area (Sect.
4   5.4). After evaluating historical trends, we additionally draw upon two simulations
5   following the 21st century RCP4.5 versus RCP8.5 global change scenarios to project
6   WUS O_3 through 2050 (Sect. 5.2). Section 6 examines how the EUS summertime O_3
7   probability distribution and pollution extremes during heat waves respond to regional
8   NO_x reductions in the past decades. Finally, we summarize in Section 7 the key drivers of
9   US surface O_3 trends and extremes and discuss model skill and shortcomings.

10

11   **2. Model and Observations**

12   **2.1 Chemistry-Climate Model Experiments.**

13   **(Table 1 about here: Model Experiments)**

14   **Table 1** summarizes meteorology, radiative forcing agents and emissions used in
15   each model experiment. All hindcast simulations include interactive
16   stratosphere-troposphere chemistry and aerosols on a cubed sphere grid with resolution of
17   approximately 200x200 km^2 (*Donner et al., 2011*), with height-dependent nudging to the
18   NCEP/NCAR reanalysis zonal and meridional winds (*Lin et al., 2012b*). Biogenic
19   isoprene emissions and lightning NO_x are tied to model meteorology (*Guenther et al.,*
20   *2006; Rasmussen et al., 2012*) and thus can respond to changes in climate, whereas soil
21   NO_x and chemical dry deposition velocities are set to a monthly climatology, with a
22   diurnal cycle applied for O_3 dry deposition. Our **BASE** simulation and two additional
23   simulations with modified emissions (**FIXEMIS** and **IAVFIRE**) were previously used to
24   interpret the causes of increasing autumnal O_3 measured at Mauna Loa Observatory in
25   Hawaii since 1974 (*Lin et al., 2014*), interannual variability of springtime O_3 (*Lin et al.,*
26   *2015a*) and the representativeness of free tropospheric O_3 measurements over the WUS
27   (*Lin et al., 2015b*). Below we describe additional simulations used in this study.
28   With anthropogenic emissions and methane held constant (**Table 1**), the FIXEMIS
29   and IAVFIRE simulations isolate the influence from meteorology and wildfire emissions,
30   respectively. In the **IAVASIA** simulation, anthropogenic emissions from East Asia
31   (15ºN-50ºN, 95ºE-160ºE) and South Asia (5ºN-35ºN, 50ºE-95ºE) are allowed to vary
32   from year to year as in **BASE**, while anthropogenic emissions in the other regions of the
33   world, global methane and wildfire emissions are held constant as in **FIXEMIS**. In the
34   **IAVCH$_4$** simulation, global methane is allowed to vary over time as in **BASE**, but with
35   anthropogenic and wildfire emissions held constant as in **FIXEMIS**. The **IAVASIA** and
36   **IAVCH$_4$** simulations thus isolate the role of rising Asian anthropogenic emissions and
37   global methane, respectively, by contrasting with the **FIXEMIS** simulation. Both **BASE**
38   and **IAVCH$_4$** simulations apply observed time-varying methane concentrations as a lower
39   boundary condition for chemistry **(Supplementary Fig.S1)**. Thus, underestimates in
40   historical methane emissions reported recently by *Schwietzke et al.* (2016) do not affect

Atmospheric
Chemistry
and Physics
Discussions

1   our results. We quantify the total contributions to surface O_3 from meteorological
2   variability, stratosphere-to-troposphere transport, pollution from foreign continents and
3   O_3 produced by global methane, lightning NO_x, wildfires and biogenic emissions with the
4   **Background** simulation, in which North American anthropogenic emissions are zeroed
5   out relative to **BASE**. We additionally draw upon two simulations with the GFDL
6   Coupled Model CM3 following the 21st century RCP global change scenarios to project
7   changes in WUS O_3 through 2050. Details of these CM3 simulations were described in
8   *John et al.* (2012).
9
10   **2.2 Anthropogenic and Biomass Burning Emissions**
11   **(Figure 1 about here: Changes in NO_x emissions)**
12   We first examine how well the emission inventories implemented in AM3_BASE
13   represent changes in regional NO_x emissions over recent decades inferred from satellite
14   measurements of tropospheric vertical column density (VCD_{trop}) of NO_2. The combined
15   record of GOME and SCIAMACHY shows that VCD_{trop} NO_2 over the highly polluted
16   region of eastern China almost tripled during 1996-2011 (**Fig.1a**). In contrast, VCD_{trop}
17   NO_2 over the EUS decreased by ~50% in the 2000s (**Fig.1b**) due to NO_x State
18   Implementation Plans (hereafter referred to as the NO_x SIP Call) and many rules that
19   tighten emission standards for mobile sources (*McDonald et al., 2012*). Similar decreases
20   occur in WUS cities, resulting from the NO_x control programs to achieve O_3 and regional
21   haze planning goals. These trends are consistent with those reported by a number of
22   recent studies (*Hilboll et al.*, 2013), including those using OMI NO_2 data (*Russell et al.*,
23   2012; *Duncan et al.*, 2016). For comparison with satellite data, we sample the model
24   archived every three hours closest to the time of satellite overpass for the SCIAMACHY
25   and GOME products we use in Figure 1 (10:00-10:30AM local time). Trends in VCD_{trop}
26   NO_2 are similar to those in NO_x emissions (orange lines versus red triangles in **Fig.1a-1b**),
27   indicating that any changes in NO_x chemical lifetime have negligible influence in our
28   model, consistent with NO_2 loss against OH being minor during the morning overpasses
29   of GOME and SCIAMACHY. The emission inventory used in AM3_BASE, from
30   *Lamarque et al.* (2010) with annual interpolation after 2000 to RCP8.5 (*Lamarque et al.*,
31   2012), mimics the opposing changes in NO_x emissions over eastern China versus the EUS
32   during 1996-2011, consistent with changes in VCD_{trop} NO_2 retrieved from the satellite
33   instruments. For comparison, the RCP4.5 interpolation for 2001-2010 in the historical
34   CMIP5 simulations analyzed by *Parrish et al.* (2014) underestimates the increase in
35   Chinese NO_x emissions by a factor of two (**Fig.1a**). We note that the levelling-off of
36   Chinese NO_x emissions after 2011 (*Duncan et al.*, 2016) is not represented in the RCP8.5
37   emission inventory used in AM3.
38   Our BASE model applies interannually-varying monthly mean emissions from
39   biomass burning based on the RETRO inventory (*Schultz et al.*, 2008) for 1970 to 1996
40   and *GFEDv3* (*van der Werf et al.*, 2010) for 1997 onwards, distributed vertically as
41   recommend by *Dentener et al. (2006)*. **Supplementary Fig. S2** illustrates the interannual

1   variability of biomass burning CO emissions from the main source regions in the

2   Northern Hemisphere over the period 1980-2014. Boreal fire emissions in Eurasia almost

3   doubled from 1980-1995 to 1996-2014, with large fires occurring more frequently in the

4   recent decade as found in recent studies for the WUS (*Dennison et al.*, 2014; *Yang et al.*,

5   2015).

6   **2.3 Ozone Observation Records and Uncertainties**

7   Long-term surface O_3 observation records were obtained at 66 rural monitoring

8   sites with 20 (1995-2014) to 27 (1988-2014) years of continuous hourly measurements

9   from the US National Park Services, the US Clean Air Status and Trends Network

10   (CASTNet), and the US EPA Air Quality System. *Cooper et al.* (2012) reported trends in

11   daytime O_3 over 1990-2010 at 53 rural sites. We investigate trends in daily maximum

12   8-hour averaged (MDA8) O_3 and expand the analysis of Cooper *et al.* (2012) using

13   additional data to 2014 and including 13 additional sites with measurements begun in

14   1991-1995. All sites have at least 20 years of data. If a site has less than 50% data

15   availability in any season then that particular season is discarded. The trend is calculated

16   separately for the 5th, 50th and 95th O_3 percentiles for each season through ordinary linear

17   least-square regression. Statistics are derived for the slope of the linear regression in units

18   of ppb yr^{-1}, the range of the slope with a 95% confidence limit (not adjusted for sample

19   autocorrelation), and the p-value indicating the statistical significance of the trend based

20   on a two-tailed *t* test.

21   **(Figure 2 about here: Measurement uncertainties)**

22   A cross-site consistency analysis was performed to determine robust changes in

23   the time evolution of O_3 over the WUS during 1988-2014 (**Fig.2**). The monitor at

24   Yellowstone National Park was moved 1.5 km from the Lake Yellowstone site to the

25   Water Tank site in 1996. While the local transport patterns are slightly different for the

26   two sites, using MDA8 data from the well-mixed midday period minimizes the

27   differences (*Jaffe and Ray, 2007*). Observed O_3 interannual variations show large-scale

28   similarity across sites over the Intermountain West except for the earlier period

29   1989-1990. During this period, observations at Yellowstone and Rocky Mountain

30   National Parks show low-O_3 anomalies that do not appear at other sites but there is no

31   change in measurement technique. *Jaffe and Ray* (2007) suggest this represents

32   large-scale variations in background O_3 that are seen in common at these two parks.

33   However, analysis of meteorological fields and model diagnostics does not reveal any

34   obvious transport anomaly influencing O_3 variations at these sites in 1990 (*Lin et al.*,

35   2015a). Observations at Pinedale in January-February 1990 are also anomalously low

36   relative to Grand Canyon (GRC474), Centennial (CNT169), and Gothic (GTH161).

37   These anomalous data at the beginning of measurement records can substantially

38   influence trends calculated from short records. For example, *Cooper et al.*, (2012) found

39   a summertime O_3 increase of 0.42±0.30 ppb yr^{-1} at Yellowstone over 1990-2010.

40   Removing 1990, we find a weaker increase of 0.28±0.27 ppb yr^{-1} (**Fig.2b**). Removing

Atmospheric
Chemistry
and Physics
Discussions

1 1990 at Rocky Mountain resulted in a weaker springtime O_3 increase of 0.29±0.17 ppb

2 yr^{-1} compared to 0.43±0.23 ppb yr^{-1} over 1990-2010 (**Fig.2c**). To assess robust O_3

3 changes, we thus remove these apparently uncertain measurements in 1990 from the

4 subsequent analysis.

5

6 **2.4 Model Baseline Sampling Approach**

7   **(Figure 3 about here: Influence of baseline sampling)**

8   Springtime O_3 observations at WUS high-elevation sites ($\geq$ 1.5 km a.s.l.) typically

9 represent baseline conditions with little influence from fresh local pollution. In a global

10 model with ~200x200 km^2 horizontal resolution, however, these remote sites can reside

11 in the same grid cell that contains urban cities where NO_x emissions decreased over the

12 analysis period. For example, Rocky Mountain National Park (2.7 km a.s.l.) is less than

13 100 km from the Denver Metropolitan area in Colorado. This limitation of large-scale

14 models in resolving urban-to-rural gradients and sharp topography results in an artificial

15 offset of increased baseline O_3 at remote sites by decreased urban pollution within the

16 same model grid cell. Thus, coarse-resolution models are often unable to reproduce the

17 observed O_3 increases at the high-elevation sites representative of remote baseline

18 conditions (**Figs. 3a vs. 3b**), as found in many prior modeling analyses (e.g., *Parrish et al.*,

19 2014; *Strode et al.*, 2015 and references therein). This limitation can be addressed by

20 using a baseline selection procedure to identify conditions for sampling the model to

21 avoid model artifacts caused by poor spatial resolution, as described below.

22   All measurements presented in this study are unfiltered. We implement a set of

23 regional CO-like tracers, with a 50-day exponential decay lifetime and surface emissions

24 constant in time from each of four northern mid-latitude source regions (*Lin et al.*, 2014).

25 We use these CO-like tracers to bin modeled O_3 according to the dominant influence from

26 different continental air regimes. To represent observed baseline conditions at

27 intermountain sites, we sample AM3 at 700 hPa (~3 km a.s.l.) and filter the O_3 data in the

28 BASE simulation to remove the influence from fresh local pollution. Specifically, our

29 filter excludes days when the North American CO tracer (NACOt) exceeds the 67th

30 percentile for each season. This procedure yields higher calculated baseline O_3 trends

31 (**Fig.3c**), bringing it closer to observations (**Fig.3a**). When sampled at 700 hPa without

32 filtering (**Fig.3d**), AM3_BASE gives statistically significant O_3 increases but the rate of

33 increase is ~0.1 ppb yr^{-1} weaker than with filtering. With North American anthropogenic

34 emissions shut off, the model simulates significant O_3 increases that are similar at the

35 surface (**Fig.3e**) and at 700 hPa (**Fig.3f**). This finding indicates that the BASE model

36 underestimate of O_3 increases when sampled at the surface (**Fig.3b**) reflects an excessive

37 offset from domestic pollution decreases in the model relative to observed conditions, as

38 opposed to insufficient mixing of free tropospheric O_3 to the surface. As individual sites

39 display observed trends falling in between the filtered model, and those sampled at the

40 surface versus at altitude, we can use the model to interpret which sites are most

41 frequently sampling baseline versus influenced by North American anthropogenic

Atmospheric
Chemistry
and Physics
Discussions

1 emissions. For consistency, in the subsequent analysis we apply the model baseline
2 sampling approach to all WUS sites with elevations greater than 1.5 km altitude. In the
3 EUS, where the terrain and monitor elevations are much lower than in the west and
4 observed O_3 trends are largely controlled by regional emission changes, we always
5 sample the model at the surface without applying data filtering.

6

7 **3. Global Distribution of Lower Tropospheric O_3 Trends**
8 **3.1 Global O_3 Burden and Distribution of Trends**

9 **(Figure 4 about here: Global distribution)**

10 We begin by examining the global distribution of lower tropospheric O_3 trends over
11 1988-2014 from the BASE simulation (**Fig.4**) and center our discussion on the
12 differences between the surface and free troposphere (~700 hPa), with implications for
13 understanding the impact of trends in hemispheric baseline O_3 on surface air quality. The
14 model indicates that surface MDA8 O_3 levels in Asia have increased significantly by
15 1.5-2.5 ppb yr^{-1} in the 95th percentile (**Fig.4a-b**) and by 1-2 ppb yr^{-1} in the median values
16 (**Fig.4c-d**), with the largest increases occurring in Southern Asia during spring and over
17 Eastern China during summer. In contrast, there is a marked decrease in surface MDA8
18 O_3 in WUS cities, throughout the EUS and in central Europe, particularly at the high
19 percentiles and during summer. The increase in surface O_3 over Asia and decreases over
20 the US and Europe are consistent with changes in regional emissions of O_3 precursors
21 over this period (**Fig.1**).
22 Over Southeast Asia (south of 30ºN) during spring, earlier springtime O_3
23 photochemical production at lower latitudes coupled with active frontal transport (*Liu et
24 al.*, 2002; *Carmichael et al.*, 2003; *Lin et al.*, 2010) leads to a comparable or even greater
25 increase of O_3 in the free troposphere than at the surface (**Figs. 4c vs. 4e**). In contrast,
26 over Central East China during summer the simulated trends of O_3 in the free troposphere
27 are at least a factor of three weaker than in surface air (**Fig.4d vs. 4f**), consistent with
28 analysis of MOZAIC aircraft data over Beijing in 1995-1999 versus 2003-2005 (*Ding et
29 al.*, 2008). Mean O_3 at 700 hPa above parts of North America and Europe show little
30 change in summer or even increase during spring in the model, similar to the trends at
31 500 hPa (**Fig.S3**), despite the significant decreases in surface air. The global tropospheric
32 O_3 burden in the BASE simulation increases by approximately 30 Tg over the past 35
33 years (**Fig.5a**), attributed mainly to changes in anthropogenic emissions. Over the
34 2004-2015 OMI/MLS satellite era, however, meteorological variability contributes
35 approximately half to the total simulated decadal trends of O_3 burden (**Fig.5a**).

36

37 **3.2 Comparison of observed and simulated O_3 trends in Asia**

38 **(Figures 5 and 6 about here)**

39 Long-term O_3 observations are very sparse in Asia, making it difficult to evaluate
40 modeled O_3 trends. We compile available measurements from the published literature;

Atmospheric
Chemistry
and Physics
Discussions

1   including ozonesonde profiles at Hong Kong (2000-2014; http:/woudc.org) and Hanoi
2   (2005-2015; SHADOZ, *Thompson et al.*, 2007), MOZAIC aircraft profiles collected on
3   summer afternoons in the boundary layer (below 1250 m altitude) over Beijing for
4   1995-2005 (*Ding et al.*, 2008), ground-based measurements at Mt. Tai (1.5 km a.s.l.) in
5   Central Eastern China for July-August 2003-2015 (*Sun et al.*, 2016), at the GAW stations
6   - Shangdianzi north of Beijing for 2004-2014 (*Ma et al.*, 2016) and Mt. Waliguan (3.8 km
7   a.s.l.) in the Tibetan Plateau for 1994-2013 (*Xu et al.*, 2016), at Taiwan for 1994-2007
8   (*Y-K Lin et al.*, 2010), South Korea for 1990-2010 (*Lee et al.*, 2014), Mt. Happo (1.9 km
9   a.s.l.) in Japan for 1991-2011 (*Tanimoto*, 2009; *Parrish et al.*, 2014), and a coastal site at
10 Hong Kong in Southern China for 1994-2007 (*T Wang et al.*, 2009).

11   We first evaluate observed and simulated annual trends of O_3 over 900-600 hPa at
12 Hanoi (21°N, 106°E) and Hong Kong (22°N, 114°E) ozonesonde sites in Southeast Asia
13 (**Fig.5b-5c**), where our model indicates the greatest free tropospheric ozone increases
14 (**Fig.4e**). The ozonesonde frequency is 4 profiles per month at Hong Kong and only 1-2
15 profiles per month at Hanoi. To determine the representativeness of O_3 trends derived
16 from these sparse measurements, we compare observations and model results co-sampled
17 on sonde launch days with the 'true average' determined from O_3 fields archived every
18 three hours from the model, as in our prior work for WUS sites (*Lin et al.*, 2015a; *Lin et
19 al.*, 2015b). The trends are generally consistent between the sonde data, model
20 co-sampled and 'true average' results for Hong Kong, with a total increase of ~15% from
21 2005 to 2014. However, our analysis indicates that sampling deficiencies may influence
22 the trends derived from ozonesondes at Hanoi recently reported by *Zhang Y. et al.* (2016).
23 Observations at Hanoi show an apparently rapid O_3 increase of 30% from 2005 to 2014.
24 AM3_BASE sampled sparsely as in the ozonesondes captures the observed variability (r^2
25 = 0.7), whereas the 'true average' over this period indicates the trend is only half of that
26 observed. Over the short period 2005-2014, interannual variability of O_3 resulting from
27 wildfire emissions and meteorology in IAVFIRE is as large as the total O_3 change in
28 BASE. Over the entire 1980-2014 period, the BASE model 'true average' simulates an O_3
29 increase of ~30%.

30   Expanding the comparison to a suite of sites across East Asia (**Fig. 6**), we find that
31 AM3_BASE captures the key features of O_3 trends in Asia, including their seasonal to
32 regional variations, summertime increases (1-2 ppb yr^{-1}) in Central Eastern China where
33 NO_x emissions have approximately tripled since 1990 (**Fig.1a**), and springtime increases
34 (0.5 ppb yr^{-1}) observed at Taiwan and Mt. Happo driven by pollution outflow from the
35 Asian continent. Note that to place the trends derived from the short observational
36 records into a broader context we show the 20-year trends over 1995-2014 from the
37 model, except for South Korea (1990-2010) and Happo Japan (1991-2011). We match the
38 time period in the model with observations at these two sites because AM3 shows weaker
39 O_3 increases when data for the recent years are included, which likely reflects the
40 offsetting effects from regional emission reductions in South Korea and Japan. Parrish *et
41 al*. (2014) found that three chemistry-climate model simulations underestimated the

Atmospheric
Chemistry
and Physics
Discussions

observed O_3 increase at Mt. Happo by at least a factor of four. This discrepancy partly reflects the limitation of global models in resolving observed baseline conditions at Mt. Happo, as occurs at WUS sites (Sect. 2.4). Sampling our model at 700 hPa and focusing on data that are strongly influenced by outflow from the East Asian continent (Chinese CO tracer > 67th percentile), we find an O_3 increase of 0.48 ± 0.13 ppb yr^{-1} at Mt. Happo (**Fig.6b**), approximating the observed increase of 0.76 ± 0.35 ppb yr^{-1}. The observed and simulated trends are not statistically different given the overlapping confidence limits. The larger confidence limit (uncertainty) derived from the Happo observations reflects the measurement inconsistency before 1998 and instrumental problems after 2007 (*Tanimoto et al.*, 2016). We conclude that the ability of GFDL-AM3 to reproduce the marked increases of O_3 pollution in Asia lends confidence in its application to assess the global impacts of rising Asian emissions.

4. Regional and Seasonal Variability of US Surface O_3 Trends

We next focus our analysis on the US where dense, high-frequency, long-term, reliable measurements of surface O_3 facilitate process-oriented model evaluation. Comparisons of surface MDA8 O_3 trends over 1988-2014 at 66 rural monitoring sites across the US as observed and simulated in AM3_BASE are shown in **Figure 7** for spring, **Figure 8** for summer, and **Figure 9** for winter. The trends are calculated separately for the 5th, 50th and 95th percentiles of the O_3 concentration distribution, with larger circles on the maps indicate sites with statistically significant trends ($p<0.05$). We first discuss observations (Sect. 4.1), followed by model evaluation and trend attribution (Sect. 4.2).

4.1 Observations

(Figure 7 about here)

In spring (**Figure 7**), observations indicate spatial heterogeneity in O_3 trends across the Intermountain West, Northeast (north of 38°N), and Southeast US. At the 95th percentile (**Fig.7a**) the pattern of observed trends is homogeneous across the Northeast and Southeast US, with approximately 87% of the sites having statistically significant O_3 decreases of 0.4-0.8 ppb yr^{-1} and no sites showing a significant increase. In contrast, significant increases occur at 20% of the sites in the Intermountain West. Only Joshua Tree National Park located downwind of the Los Angeles Basin shows a significant decrease at the 95th percentile. At the 50th percentile (**Fig.7b**) there are significant O_3 decreases of 0.2-0.4 ppb yr^{-1} in the Southeast and little overall change in the Northeast, while significant increases of 0.2-0.4 ppb yr^{-1} occur at 50% of the sites in the Intermountain West. Significant springtime O_3 increases occur at all observed percentiles at Lassen Volcanic National Park in California, Great Basin National Park in Nevada, Rocky Mountain National Park and US Air Force Academy in Colorado. At the 5th percentile (**Fig.7c**) significant O_3 increases occur at most sites in the Northeast while little change and some negative trends are found in the Southeast. The observed greatest O_3

Atmospheric
Chemistry
and Physics
Discussions

1   decreases for the highest percentiles are consistent with high-temperature O_3 production
2   being more NO_x-limited (*Pusede et al.*, 2015), and thus more responsive to the decreases
3   in NO_x emissions over the past decade. The north-to-south gradient in springtime O_3
4   trends over the EUS reflects the earlier seasonal transition from NO_x-saturated to
5   NO_x-sensitive O_3 production regimes in the Southeast, where plentiful radiation in spring
6   enhances HO_x supply and biogenic isoprene emissions are turned on earlier than the
7   Northeast.

8   **(Figure 8 about here)**

9   In summer (**Figure 8**), as radiation intensifies and isoprene emissions peak
10   seasonally, the O_3 production becomes more NO_x-limited across both the Southeast and
11   Northeast US where NO_x emission controls have led to significant O_3 decreases of
12   0.8-1.8 ppb yr^{-1} in the 95th percentile and 0.4-0.8 ppb yr^{-1} in the median value (**Fig.8a-8b**).
13   In the Southeast, significant decreases have also occurred at the lowest percentiles during
14   summer (**Fig.8c**), in contrast to the weak response during spring (**Fig.7c**). Despite
15   reductions in precursor emissions in the WUS cities (**Fig.1d**), there are no significant
16   summer O_3 decreases at the intermountain sites except at Yosemite and Joshua Tree
17   National Parks for the 95th percentile. Instead, a significant summer increase of ~0.3 ppb
18   yr^{-1} occurs across the entire O_3 distribution at Yellowstone National Park. Significant
19   summer increases are found in the 5th percentile for Lassen, Mesa Verde, and Rocky
20   Mountain National Parks.

21   **(Figure 9 about here)**

22   In winter (**Figure 9**), observed O_3 increases are more common than in spring and
23   summer across the US. Notably, the wintertime O_3 increases are strongest in the lowest
24   percentiles over the EUS, indicating the influence from weakened NO_x titration as a
25   result of regional NO_x emission controls (see also *Gao et al.*, 2013; *Clifton et al.*, 2014;
26   *Simon et al.*, 2015). Some decreasing O_3 trends are found in the highest percentiles over
27   the Southeast even during winter (**Fig.9a**), similar to the Los Angeles Basin (not shown)
28   where tropical climate and year-round active photochemistry makes O_3 most responsive
29   to regional NO_x emission controls. Despite the greatest NO_x emission reductions over the
30   past decade in the central and northeast US regions, observed O_3 reductions have been
31   most pronounced in the Southeast, particularly in spring and winter.
32

33   **4.2 Model Evaluation and Attribution of Observed O_3 Trends**
34   The BASE simulation with GFDL-AM3 captures the salient features of observed O_3
35   trends over 1988-2014 at rural sites across the US: (1) the overall springtime increases
36   and the lack of significant trends in summer over the Intermountain West, (2) the
37   north-to-south gradients in O_3 trends during spring and the largest decreases in the 95th
38   percentile during summer over the EUS, (3) wintertime increases in the 5th and 50th
39   percentiles (left vs right panels in **Figs. 7 to 9**). AM3 also simulates the median
40   springtime O_3 increase of 0.32±0.11 ppb yr^{-1} over 1988-2014 (0.64±0.50 ppb yr^{-1} over

1 2004-2014) at Mount Bachelor Observatory in Oregon, consistent with the positive trends

2 (0.63 ± 0.41 ppb yr^{-1}) observed over the shorter 2004-2015 period (*Gratz et al.*, 2014).

3 These analyses imply that GFDL-AM3 represents the underlying chemical and physical

4 processes controlling the response of US surface O_3 means and extremes to changes in

5 global-to-regional precursor emissions and climate, despite mean state biases (**Figs.**

6 **S4-S5**).

7 The filtered model shows greater 95th percentile O_3 increases than observed at

8 some WUS sites (e.g., Yosemite; Grand Canyon; Canyonlands) for both spring and

9 summer (**Figs.7a,d and Fig.8a,d**), reflecting that observations at these sites sometimes

10 can be influenced by transport of photochemically aged plumes from nearby urban areas

11 and from southern California during late spring and summer. When sampled at the

12 surface, AM3 simulates small summertime O_3 decreases in the 95th and 50th percentiles

13 over the Intermountain West (**Fig.4b,d),** consistent with observations at Yosemite, Grand

14 Canyon, and Canyonlands (**Fig.8a,b**). As illustrated in **Fig.3** for spring and discussed in

15 Sect. 2.4, individual sites in the west display observed trends falling in between the

16 filtered model and those sampled at the surface versus aloft.

17 **(Figures 10 and 11 about here)**

18 We examine how US surface O_3 responds to changes in regional anthropogenic

19 emissions, hemispheric background, and meteorology by comparing O_3 trends in the

20 BASE, Background, and FIXEMIS experiments (**Figs. 10-11**). With North American

21 anthropogenic emissions shut off in the Background simulation, little difference is

22 discernable from the BASE simulation for the WUS O_3 trends during spring (first vs.

23 second rows in **Fig.10**), indicating the key role of hemispheric background driving

24 increases in springtime O_3 over the WUS. With anthropogenic emissions held constant in

25 time, FIXEMIS still shows statistically significant spring O_3 increases in the 95th

26 percentile (**Fig.10c**), approximately half of the trends simulated in BASE, for Grand

27 Canyon, Canyonlands, Mesa Verde and Rocky Mountain National Parks. Prior work

28 shows that deep stratospheric intrusions contribute to the highest observed and simulated

29 surface O_3 events at these sites (*Langford et al.*, 2009; *Lin et al.*, 2012a). Strong

30 year-to-year variability of such intrusion events (*Lin et al.*, 2015a) can confound the

31 attribution of springtime O_3 changes over the WUS to anthropogenic emission trends,

32 particularly in the highest percentile and over a short record length. Summer avoids this

33 confounding influence when stratospheric intrusions are at their seasonal minimum, as

34 evidenced by little O_3 change in FIXEMIS over the WUS (**Figs. 11c,f**). In contrast to

35 spring, the model shows larger differences in WUS O_3 trends between BASE and

36 Background during summer when the influence of North American pollution peaks

37 seasonally (**Figs.10a,d vs. 10b,e compared to Figs.11a,d vs. 11b,e**). There are significant

38 increases of 0.2-0.5 ppb yr^{-1} in the 95th and 50th percentile summer background O_3 at

39 more than 50% of the western sites (**Fig.11b,e**), offsetting the O_3 decreases resulting from

40 US NO$_x$ reductions and leading to little overall change in total observed and simulated O_3

1   at WUS rural sites during summer (**Fig.8**).

2   Over the EUS, AM3 also simulates background O_3 increases, occurring in both the
3   95th and 50th percentiles, with a rate of 0.1-0.3 ppb yr^{-1} during spring (**Fig.10b,e**) and
4   0.2-0.5 ppb yr^{-1} during summer (**Fig.11b,e**). Rising biogenic isoprene emissions
5   contribute to the EUS background O_3 increase in summer (**Fig.12a**). Based on prior
6   model estimates that springtime background O_3 is greater in the Northeast than the
7   Southeast (*Lin et al.*, 2012a; *Lin et al.*, 2012b; *Fiore et al.*, 2014), one might assume that
8   the springtime O_3 increases in the 5th percentile observed over the Northeast (**Fig.7c**) have
9   been influenced by a rising background. However, AM3 simulates homogeneous
10   background O_3 trends across the entire EUS (**Fig.10b,e**), indicating that the observed
11   north-to-south gradient in O_3 trends reflects an earlier onset of NO_x-sensitive
12   photochemistry in the Southeast as opposed to the background influence.

13   **(Figure 12 about here).**

14   A warming climate is most likely to worsen the highest O_3 events in polluted
15   regions (e.g., *Schnell et al.*, 2016; *Shen et al., 2016*). With anthropogenic emissions held
16   constant in time over 1988-2014, FIXEMIS suggests significant increases of 0.2-0.4 ppb
17   yr^{-1} in the 95th percentile summertime O_3 over the EUS (**Fig.11c**). Using self-organizing
18   map cluster analysis, Horton *et al*. (2015) identified robust increases in the occurrence of
19   summer and autumn anticyclonic circulations over eastern North America since 1990. We
20   find that biogenic isoprene emissions over this period increase significantly by 1-2% yr^{-1}
21   (10 to 20 mg C m^{-2} $summer^{-1}$) throughout the EUS in the model, consistent with
22   simulated increases in the 90th percentile JJA daily maximum temperature (**Fig. 12a-12b**).
23   We further analyze the Global Land-Based Datasets for Monitoring Climate Extremes
24   (GHCNDEX; Donat et al., 2013) and find increases in the number of warm days above
25   the 90th percentile and maximum temperature over the central and southeast US in August
26   (**Fig.12c-12d**). The trends in temperature extremes are similar between June and August,
27   but there is no significant trend in July (not shown). While changes in regional
28   temperature extremes on 20 to 30-year time series may merely reflect internal climate
29   variability (*Shepherd, 2015*), we suggest that the increased frequency of hot extremes and
30   rising isoprene emissions over the last two decades may have offset some of air quality
31   improvements in the EUS gained from regional NO_x reductions.

32

33   **5. Impacts of rising Asian emissions, methane and wildfires on western US O_3**
34   **5.1 Historical western US O_3 trends in spring**

35   **(Figure 13 about here: Time series analysis)**

36   Further indications of the factors driving baseline O_3 changes over the WUS can
37   be inferred by examining the time series at several high-elevation sites, which are most
38   frequently sampling baseline O_3 in the free troposphere during spring (Sect. 2.4). **Figure**
39   **13** shows the results, both observed and simulated, for six such monitoring sites: Great
40   Basin National Park in Nevada (2.1 km a.s.l.), Rocky Mountain National Park (2.7 km

Atmospheric
Chemistry
and Physics
Discussions

1   a.s.l.) in Colorado, US Air Force Academy (1.9 km a.s.l.) in Colorado Springs,
2   Yellowstone National Park (2.4 km a.s.l.) and Pinedale (2.4 km a.s.l.) in Wyoming, and
3   Mesa Verde National Park (2.2 km a.s.l.) in the Colorado-New Mexico-Arizona-Utah
4   four corner region. The observed median values of springtime MDA8 O_3 have increased
5   significantly at a rate of 0.2-0.5 ppb yr^{-1} over the past 20-27 years at these sites, except
6   Pinedale, where the increase in background O_3 is likely offset by the O_3 decrease due to
7   recent emission control for the large oil and gas production fields in this area
8   (http://deq.wyoming.gov/aqd/winter-ozone/resources/technical-documents/). When filtered to
9   remove the influence from fresh local pollution (Sect.2.4), AM3_BASE captures the
10   long-term trends of O_3 observed at these sites.

11   Correlating AM3 Background directly with the observations indicates that most of
12   the observed variability reflects changes in the background, with fluctuations in
13   stratospheric influence contributing to anomalies on interannual time scales (e.g., the
14   1999 anomaly, *Lin et al., 2015a*), whereas Asian influence dominates the decadal trends
15   as discussed below. The O_3 reduction resulting from US anthropogenic emission controls
16   is less than 0.1 ppb yr^{-1} (BASE minus Background) at these baseline sites. We show
17   model results for the entire 1980-2014 period for Great Basin, Rocky Mountain, and US
18   Air Force Academy to provide context for observed trends in the two most recent decades
19   (**Fig.13a**). In the 1980s when Chinese NO_x emissions (~4 Tg/yr NO) were much lower
20   than US NO_x emissions (~15 Tg/yr NO) (*Granier et al.*, 2011), there was little overall O_3
21   change over the WUS in the model. From the mid-1990s onwards, with NO_x emissions in
22   China rising steeply (**Fig.1a**) and surpassing US emissions in the 2000s, we find that the
23   O_3 trends at remote WUS sites appear to be dominated by trends of background,
24   reflecting rising emissions outside the US. Supporting the Asian influence, the regions
25   experiencing the largest springtime O_3 increases from 1981-1990 to 2003-2012 at 700
26   hPa extend from Southeast Asia to the subtropical North Pacific Ocean to the
27   southwestern US (**Fig.S6a**).

28   **(Table 2 about here: Trend attribution)**

29   **Table 2** contains a summary of the drivers of O_3 trends in the model at seven
30   CASTNet sites with a significant springtime O_3 increase observed over the period
31   1988-2012. Here we focus our attribution analysis on the period 1988-2012 (instead of
32   1988-2014) because the IAVASIA and $IAVCH_4$ simulations only extend to 2012.
33   Meteorology varies from year to year in all experiments. Thus, we quantify the
34   contributions from rising Asian emissions in IAVASIA, global methane in $IAVCH_4$, and
35   wildfire emissions in IAVFIRE by subtracting out the slope of the linear regression of
36   seasonal O_3 means in FIXEMIS. Simulated O_3 with anthropogenic emissions varying in
37   both South and East Asia (red boxes in **Fig.1c**) but held constant elsewhere gives
38   statistically significant increases of 0.1-0.2 ppb yr^{-1} ($p \leq 0.01$; IAVASIA minus FIXEMIS
39   in **Table 2**), consistent with trends of 0.2 ppb yr^{-1} estimated from HTAP phase 1
40   multi-model sensitivity experiments in which Asian emissions were reduced by 20%

Atmospheric
Chemistry
and Physics
Discussions

(*Riedmiller et al., 2009*). This Asian influence can explain 50-65% of the total background O_3 increases in spring (Background in **Table 2**).

With only methane varying, the model trends are less than 0.1 ppb yr^{-1} ($IAVCH_4$ minus FIXEMIS), accounting for an average of 15% of the total background increases. The contribution from wildfire emissions during spring is of minor importance, as evidenced by the small differences between FIXEMIS and IAVFIRE (**Table 2**). A stratospheric O_3 tracer (O_3Strat) in AM3 (*Lin et al.*, 2012a; *Lin et al.*, 2015a) demonstrates a positive but insignificant trend in stratospheric O_3 transport to the sites. We examine the trends of lower tropospheric O_3 at these sites when transport conditions favor the import of Asian pollution into western North America, as diagnosed by East Asian CO tracer (EACOt) exceeding the 67th percentile for each spring. Similar to the conclusion of *Lin et al.*, (2015b), we find that the rate of O_3 increase under strong transport from Asia is greater by 0.05-0.1 ppb yr^{-1} than without filtering in the Background simulation. Filtering the IAVASIA simulation for Asian influence also results in greater O_3 increases than filtering for baseline conditions (**Table 2**).

Increasing O_3 from rising Asian emissions can also influence trends of O_3 downwind of the Los Angeles Basin during spring. For instance, Cooper *et al.* (2012) found that O_3 measured in Joshua Tree National Park shows an increase of 0.31±0.25 ppb yr^{-1} in spring over 1990-2010, despite significant improvements in O_3 air quality in the Los Angeles Basin (*Warneke et al.*, 2012). An extended O_3 record to 2014 shows a decline in the 95th percentile O_3 in Joshua Tree National Park for both spring and summer (**Figs. 7-8**), whereas the 5th percentile continues to increase in spring and there is no significant trend in the median. Sampling the model background simulation at this site indicates rising background (0.31±0.14 ppb yr^{-1}). Aircraft measurements in May-June 2010 indicate the presence of Asian pollution layers 2 km above Joshua Tree National Park with distinct sulfate enhancements coincident with low organic mass (*Lin et al.*, 2012b), supporting the conclusion that rising Asian emissions can contribute to trends of O_3 observed in this region. Yosemite National Park (1.6 km a.s.l.) and Chiricahua National Monument (1.5 km a.s.l.) are also influenced by increases in Asian emissions and concurrent decreases in California. Ozone observed at Yosemite show an increase from 1995 to around 2012 (0.37±0.32 ppb yr^{-1}; **Fig.S7**), which the model attributes to rising background (primarily from trends of Asian emissions; **Table 2**), but observations have remained constant since then, reflecting an offset by O_3 decreases in California (**Fig.4**).

5.2 Projecting western US springtime O_3 for the 21st Century

(Figure 14 about here: Future Projections).

Under the RCP8.5 scenario, Chinese NO_x emissions are projected to peak in 2020-2030, reflecting an increase from year 2010 by ~50% (**Fig.1a),** and global methane increases by ~60% from 2010 to 2050 (**Fig.S1**). Under the RCP4.5 scenario, in contrast, NO_x

Atmospheric
Chemistry
and Physics
Discussions

1   emissions in China change little over 2010-2030 and global methane remains almost
2   constant from 2010 to 2050. NO_x emissions in the US decrease through 2050 under both
3   RCP4.5 and RCP8.5, by ~40% from 2010. We examine the extent to which these changes
4   influence trends of springtime O_3 over the WUS. A number of studies have examined
5   future US O_3 changes under the RCPs (e.g., *Gao et al.*, 2013; *Clifton et al.*, 2014; *Pfister
6   et al.*, 2014; *Fiore et al.*, 2015; *Barnes et al.*, 2016). However, as discussed earlier in this
7   study the trends of O_3 in the model when sampled near the surface are overwhelmingly
8   dominated by the trends of US anthropogenic emissions. Thus, the future O_3 changes
9   estimated by these prior studies do not represent baseline conditions, particularly the
10 response to rising Asian emissions. In **Fig. 14** we show changes of free tropospheric (700
11 hPa) O_3 relative to 2010 over the WUS in the CM3 future simulations under RCP8.5
12 versus RCP4.5. Historical hindcasts and observations averaged from Lassen, Great Basin,
13 and Rocky Mountain are also shown for context. Under RCP4.5, springtime O_3 over the
14 WUS shows little overall change over 2010-2050. Under RCP8.5, in contrast, springtime
15 O_3 over the WUS increases by ~10 ppb from 2010 to 2030 and remains almost constant
16 from 2030 to 2050, consistent with the projected trend in Asian anthropogenic emissions
17 and global methane.
18
19 **5.3 Trends and variability of western US O_3 in summer**

20 **(Figure 15 about here: Yellowstone)**

21   Yellowstone National Park is the only site with statistically significant summer
22 O_3 increases observed across all percentiles (**Fig.8a-8c**). The 1988-2012 trends for the
23 median from observations and model simulations are summarized in **Figure 15a**.
24 Observations show an increase of 0.32±0.18 ppb yr^{-1} for JJA, with a greater rate of
25 increase in June (0.38±0.25 ppb yr^{-1}) than in July-August (0.26±0.18 ppb yr^{-1}).
26 AM3_BASE sampled at 700 hPa and filtered for baseline conditions (hatched pink bar in
27 **Fig.15a**) captures the observed increase. Without baseline filtering (solid pink bar), North
28 American emission reductions offset almost 50% of the O_3 increase at Yellowstone in the
29 model, causing the model to underestimate the observed O_3 trend. The model attributes
30 much of the observed summertime O_3 increase at Yellowstone to rising Asian emissions,
31 with IAVASIA simulating an O_3 increase of 0.31±0.19 ppb yr^{-1} under baseline conditions,
32 increasing to 0.42±0.23 ppb yr^{-1} when under conditions of Asian influence (EACOt ≥ 67th
33 percentile). The stronger increase measured in June than in July-August is consistent with
34 the seasonality of pollution transport from Asia. In contrast, changes in methane,
35 wildfires and meteorology over this period are of minor importance for the decadal O_3
36 trends at Yellowstone.
37   Enhanced wildfire activity in hot and dry weather is thought to be a key driver of
38 interannual variability of surface O_3 in the Intermountain West from summer into fall
39 (*Jaffe et al.*, 2008; *Pfister et al.*, 2008; *Jaffe*, 2011). However, hot and dry conditions also
40 facilitate the buildup of O_3 produced from regional anthropogenic emissions, which can

Atmospheric
Chemistry
and Physics
Discussions

complicate the unambiguous attribution of observed O_3 enhancements. Using August data at Yellowstone as an example, we isolate the relative contribution of these two processes to observed O_3 with the IAVFIRE versus FIXEMIS experiments (**Fig.15b**; note that here we sample AM3 at the surface to account for any influence from boundary layer mixing depths). Even with wildfire emissions held constant in time, FIXEMIS captures much of the observed year-to-year variability of August mean O_3 at Yellowstone (r=0.67). IAVFIRE with time-varying fire emissions only moderately improves the correlations (r = 0.75). FIXEMIS also captures the observed O_3 increase from the early 1990s to around 2002, likely reflecting warmer temperature and deeper mixing depths pulling down more baseline O_3 to the surface. Over the entire 1988-2014 (or 1980-2014) period, IAVFIRE gives ~0.1 ppb yr^{-1} greater O_3 trends in August than FIXEMIS, consistent with an overall increase in boreal wildfire activity **(Fig.S2 and Fig.S6b).**

(Figure 16 about here: Wildfires)

Figure 16 shows year-to-year variability in surface MDA8 O_3 enhancements from wildfires during summer, as diagnosed by the differences between IAVFIRE and FIXEMIS. The results are shown for individual months, since fires are highly episodic. During the summers of 1998, 2002, and 2003, biomass fires burned a large area of Siberia and parts of the North American boreal forests, raising carbon monoxide burden across the Northern Hemisphere as detected from space (*Jaffe et al.*, 2004; *van der Werf et al.*, 2010; *Yurganov et al.*, 2005). Long-range transport of the Siberian fire plumes resulted in 2-6 ppb enhancements in surface MDA8 O_3 at the US west coast and in parts of the Intermountain West according to AM3. The model calculates enhancements in monthly mean MDA8 O_3 of up to 8 ppb from the intense wildfire events in Northern California during July 2008 (*Huang et al.*, 2013; *Pfister et al.*, 2013), over Texas-Mexico during June 2011 (*Y Wang et al.*, 2015), and in Wyoming-Utah during August 2012 (*Jaffe et al.*, 2013). The AM3 estimates are roughly consistent with analysis of boundary layer aircraft data with and without fire influences (as diagnosed by CH_3CN) during June 2008 over California (*Pfister et al.*, 2013).

While fires during hot and dry summers clearly result in enhanced O_3 at individual sites for some summers, the ability of AM3 with constant fire emissions to simulate variability of O_3 (±8 ppb) for a high (e.g., 1988; 2002; 2006) versus low (e.g., 1997; 2009) fire activity year (**Fig.15b**) indicates that biomass burning is not the primary driver of summer O_3 interannual variability. Year-to-year variability of JJA mean MDA8 O_3 observed at Yellowstone is strongly correlated (r > 0.6) with observed large-scale variations in JJA mean daily maximum temperature across the Intermountain West and the Great Plains (**Fig.15c**). Correlations for other ground stations show a similar large-scale feature. Similar to the conclusion from *Zhang L. et al.* (2014), our analysis indicates that the correlation between O_3 and biomass burned reported by *Jaffe et al.* (2008, 2011) at rural sites reflects common underlying correlations with temperature rather than a causal relationship of fire on O_3. At remote mountain sites (e.g.,

Atmospheric
Chemistry
and Physics
Discussions

Open Access

EGU

1   Yellowstone), warmer surface temperatures lead to deeper mixed layers that facilitate

2   mixing of free tropospheric air with higher O_3 concentrations down to the surface

3   (*Brown-Steiner and Hess*, 2011). At sites nearby sources of air pollution, hot conditions

4   enhance regional O_3 production and orographic lifting of urban pollution to mountain-top

5   sites during daytime, as occurs at Rocky Mountain National Park located downwind of

6   the Denver Metropolitan area during summer (**Sect. 5.4**). Baker et al. (2016) found that

7   reactive volatile organic compound (VOC) emissions from fires can enhance O_3

8   production in NO_x-rich urban areas. Evaluating these impacts needs high-resolution

9   models and better treatment of fire plumes.

10

11   **5.4 Ozone Trends in the Denver Metropolitan Area**

12   **(Figure 17 about here: Denver)**

13   Efforts to improve air quality have led to a marked decrease in high-O_3 events in

14   the Los Angeles Basin as illustrated with annual 4th highest MDA8 O_3 at Crestline – a

15   regionally representative monitor operated continuously from 1980 to present (**Fig.17a**).

16   In striking contrast, the 4th highest MDA8 O_3 in the Denver Metropolitan area shows little

17   change over the past decades, despite significant reductions in NO_x (**Fig.1**) and CO

18   emissions (-80% from 1990-2010; *Cooper et al.*, 2012). Recent field measurements

19   indicates that VOC emissions from increasing oil and natural gas operations are an

20   important source of O_3 precursors in the Denver-Julesberg Basin (*Gilman et al.*, 2013;

21   *Halliday et al.*, 2016; *McDuffie et al.*, 2016). However, total VOC emissions in Denver

22   may not be increasing over time due to the marked reductions in VOC emissions from

23   vehicles (*Bishop and Stedman*, 2008; 2015). We seek insights into the causes of the lack

24   of significant O_3 responses to emission controls in Denver by separately analyzing trends

25   in spring and summer (**Fig.17b-17c**).

26   The ~200x200 km^2 AM3 simulations are not expected to resolve the urban-to-rural

27   differences between Rocky Mountain National Park and the Denver Metropolitan area.

28   However, if observed O_3 variability in Denver correlates with that at remote sites in the

29   Intermountain West, then model attribution for the remote sites can be used to infer

30   sources of observed O_3 in Denver. This is demonstrated in **Fig.17b** for spring using data

31   at three representative sites in Denver: Rocky Flats North, National Renewable Energy

32   Lab (NREL), and Welby with continuous measurements since the early 1990s.

33   Year-to-year variability of median MDA8 O_3 at these sites during spring correlates

34   strongly with that in Great Basin National Park ($r = 0.7$) - a fairly remote site in Nevada

35   not influenced by urban emissions in Denver. Median spring O_3 observations in Denver

36   increased significantly by ~0.3 ppb yr^{-1} similar to the rate of increase in Great Basin

37   National Park which the model attributes to rising background (**Fig.13a**), implying that

38   the tripling of Asian emissions since 1990 also raised mean springtime O_3 in the Denver

39   Metropolitan area. Trends in the 95th percentile are statistically insignificant.

40   During summer, changes in regional emissions and temperature have the greatest

1   impacts on the highest observed O_3 concentrations in polluted environments. **Fig.17c**
2   shows times series of July-August 95th percentile MDA8 O_3 in Denver, together with the
3   distribution of daily maximum temperature. In every year since 1993 the highest summer
4   MDA8 O_3 observed at these sites exceeds the 70 ppb NAAQS level. There is a small
5   negative trend that is swamped by large interannual variability. The summers with the
6   highest observed O_3 coincide with those with the highest observed temperatures, such as
7   1998, 2003, 2007, 2011 and 2012. During these summers, enhancements of MDA8 O_3
8   were also recorded at Rocky Mountain National Park, reflecting enhanced lifting of
9   pollution from Denver under warmer conditions (*Brodin et al.*, 2010). Appling quantile
10 regression (e.g., *Porter et al.*, 2015) to daily observations at Rocky Flats North over
11 1993-2015, we find a 2 ppb $°C^{-1}$ sensitivity of 95th percentile July-August O_3 to changes
12 in maximum daily temperature. We suggest that the substantial increases in extreme heat
13 occurrence over central North America over the last two decades, as found by *Horton et*
14 *al*. (2015), contribute to raising summer O_3 in Denver, which offsets O_3 reductions that
15 otherwise would have occurred due to emission controls in Denver. Potential shifts in the
16 O_3 photochemistry regime can also contribute to trends of summer O_3 in Denver,
17 although advancing this knowledge would require a high-resolution air quality model.
18
19 **6. Summer O_3 pollution extremes over the eastern US**

20 **(Figure 18 about here: Interannual Variability)**

21 We discuss in this section interannual variability and long-term changes in summer O_3
22 over the EUS, where air stagnation and high temperatures typically yield the highest O_3
23 observed in surface air (e.g., *Jacob and Winner 2009*). Evaluating the ability of models to
24 simulate the high-O_3 anomalies during large-scale heat waves is crucial to establishing
25 confidence in the model projection of pollution extremes under a warming climate.
26 **Figure 18** shows comparisons of July mean MDA8 O_3 at one regionally representative
27 site – the Pennsylvania State CASTNet site - as observed and simulated by the model.
28 With time-varying emissions, the BASE model simulates an O_3 decrease (-0.45±0.32 ppb
29 yr^{-1}) consistent with observations (-0.67±0.33 ppb yr^{-1}), and captures the observed July
30 mean O_3 interannual variability (r = 0.82) that is correlated with large-scale variations in
31 daily maximum temperature (r = 0.57). In particular, the O_3 pollution extremes are
32 successfully simulated during the EUS summer heat waves of 1988, 1999, 2002, 2011
33 and 2012 (*Leibensperger et al.*, 2008; *Fiore et al.*, 2015; *Jia et al.*, 2016). Year-to-year
34 variations in such air stagnation events can explain 30% of the total observed O_3
35 variability (r = 0.55), as inferred by FIXEMIS with constant anthropogenic emissions. If
36 US anthropogenic emissions remained at 1990s levels (as in FIXEMIS), then anomalies
37 in July mean MDA8 O_3 would have been 10 ppb greater during the 2011 and 2012 heat
38 waves. *Loughner et al.* (2014) found that half of the days in July 2011 would have been
39 classified as O_3 exceedance days for much of the mid-Atlantic region if emissions had not
40 declined.

Atmospheric
Chemistry
and Physics
Discussions

1   **(Figure 19 about here: Changes in O_3 distribution)**

2   **Figure 19a** compares the probability density functions of MDA8 O_3 at 40 EUS
3   surface sites for JJA in the pre-NO_x SIP Call (1988-2002) versus post-NO_x SIP Call
4   (2003-2014) periods and during the extreme heat waves of 1988 versus 2012. Following
5   the NO_x SIP Call, observed JJA MDA8 O_3 over the EUS manifested a downward shift in
6   the probability distribution (black vs. gray lines in **Fig.19a**), with the median value
7   declining by 9 ppb and the largest decreases occurring in the upper tails, leading to
8   weaker day-to-day O_3 variability and a narrower O_3 range (standard deviation σ
9   decreased from 16.4 to 12.9 ppb). Using fewer data in 1995-1998 vs. 2002-2005, *Rieder*
10 *et al.* (2015) also noted a shift in the O_3 distribution. These observed O_3 changes driven
11 by regional NO_x reductions are even more prominent when comparing the heat waves of
12 1988 versus 2012 (red vs. brown lines in **Fig.19a**): σ = 22.3 vs. 13.4 ppb and median
13 value μ= 68.6 vs. 52.2 ppb. Regional emission reductions significantly alleviated the O_3
14 buildup during the 2012 heat wave relative to earlier heat waves.

15 **Fig.19b** shows the corresponding comparisons using the results from AM3 BASE.
16 Despite the high mean model bias (~20 ppb), AM3 captures the overall structure of the
17 changes in the surface O_3 distributions and thus the response of surface O_3 to the NO_x SIP
18 Call, including the reductions of high-O_3 events during the heat wave of 2012 compared
19 to 1988. Nevertheless, there is a noticeable difference between the observations and
20 simulations in the shape of MDA8 O_3 probability distributions for summer 1988,
21 particularly in the upper tail of the distribution (red lines in **Figs.19a vs. 19b**). One
22 possible explanation for this bias is that the 1988 heat wave coincided with severe
23 drought conditions (*Seager and Hoerling*, 2014), which can effectively "turn off" the O_3
24 deposition sink to vegetation, leading to a substantial increase in surface O_3
25 concentrations as found during the 2003 European heat wave (*Solberg et al.*, 2008;
26 *Emberson et al.*, 2013), whereas AM3 does not include interannually varying dry
27 deposition velocities for O_3. Quantile mapping can be applied to correct systematic
28 distributional biases in surface O_3 compared to observations (*Rieder et al., 2015*), but this
29 approach has limitations if there are structural biases in the O_3 distribution due to missing
30 physical processes in the model.

31 Travis et al. (2016) suggest that the National Emission Inventory (NEI) for NO_x
32 from the US EPA is too high nationally by 50% and that decreasing US NO_x emissions by
33 this amount corrects their model bias for boundary layer O_3 by 12 ppb in the Southeast
34 for summer 2013, while surface MDA8 O_3 in their model is still biased high by 8±13 ppb,
35 which the authors attribute to excessive boundary layer mixing. US NO_x emissions in the
36 emission inventory used in AM3 (Sect. 2.2) are approximately 15% lower than those
37 from the NEI. The 35% decrease in NO_x emissions from the pre-NO_x SIP Call to the
38 post-NO_x SIP Call in the model reduces mean O_3 by 8 ppb in the EUS, implying that the
39 NO_x emission bias could correct 40% of our model mean bias of ~20 ppb. These
40 estimates support the idea that the common model biases in simulating surface O_3 over
41 the Southeast US (e.g., *Fiore et al.*, 2009) may partly reflect excessive NO_x emissions.

1   Some of the positive O_3 biases could be also due to the averaging over a deep vertical box
2   in the model surface layer that can't resolve near-surface gradients.
3
4   **7. Conclusions**
5   **(Figure 20 about here: 2003-2012 minus 1981-1990)**
6   Through a comprehensive analysis of interannual variability and long-term trends in
7   sources of O_3 over the past 35 years, we have discussed the key factors controlling US O_3
8   pollution. In **Fig.20**, we summarize the overall statistics, drawing upon the decadal mean
9   MDA8 O_3 changes from 1981-1990 to 2003-2012 in the AM3 BASE and sensitivity
10 simulations. The changes in BASE are: over the WUS 4.3±1.8 ppb for spring and 1.6±1.2
11 ppb for summer; over the Northeast -1.8±1.7 ppb for spring and -6.0±2.0 ppb for summer;
12 over the Southeast -3.9±1.4 ppb for spring and -7.5±1.6 ppb for summer. Increasing O_3
13 under BASE for the WUS coincides with an increase of background O_3 by 6.3±1.9 ppb
14 for spring and 4.2±2.0 ppb for summer. Under conditions of strong transport from Asia,
15 the background trend rose to 7.6±2.2 ppb for spring and 6.0±2.1 ppb for summer (green
16 dots in **Fig.20**). The background O_3 increase in the WUS reflects the contribution from
17 increases in Asian anthropogenic emissions (accounting for 50% of background increase
18 in spring; 52% in summer), rising global methane (13% in spring; 23% in summer), and
19 variability in biomass burning (6% in spring; 12% in summer; with the meteorological
20 influence subtracted out). We conclude that rising Asian anthropogenic emissions are the
21 major driver of increasing background O_3 over the WUS for both spring and summer.
22 Methane increases contribute to a much lesser extent than rising Asian emissions.
23   Our synthesis of available observations and model simulations indicates that
24 surface and free tropospheric O_3 over East Asia has increased by 1-2 ppb yr^{-1} since 1990
25 (i.e., 25-50 ppb over 25 years), with significant implications for regional air quality and
26 global tropospheric O_3 burden (**Figs.4-6**). We find 0.2-0.5 ppb yr^{-1} increases in median
27 springtime MDA8 O_3 measured at 50% of sixteen WUS rural sites, with 25% of the sites
28 showing increases across the entire O_3 concentration distribution (**Fig. 7**). While many
29 prior studies show that global models have difficulties simulating O_3 increases at WUS
30 sites, we reconcile observed and simulated O_3 trends with a novel baseline sampling
31 approach (**Figs.3 and 13**). The ability of GFDL-AM3 to reproduce observed O_3 increases
32 at WUS sites lends confidence in its application for attribution of observed trends. The
33 tripling of Asian NO_x emissions since 1990 contributes to as much as 65% of modelled
34 springtime background O_3 increases (0.3-0.5 ppb yr^{-1}) over the WUS, outpacing O_3
35 decreases resulting from U.S. domestic emission controls (**Table 2 and Fig.10**).
36 Springtime O_3 observed in the Denver and Colorado Springs metropolitan areas has
37 increased at a rate similar to those at remote rural sites (**Fig. 17b**). We further show that
38 mean springtime O_3 above the WUS would increase by ~10 ppb from 2010 to 2030 under
39 the RCP8.5 global change scenario but would remain constant throughout 2010 to 2050
40 under the RCP4.5 scenario (**Fig.14**).

Atmospheric
Chemistry
and Physics
Discussions

1   During summer, rising Asian anthropogenic emissions over 1988-2014
2   approximately offset the effects of US domestic emission controls, leading to weak or
3   insignificant O_3 trends observed at most WUS rural sites (**Figs.8 and 11**). Rising Asian
4   emissions contribute to observed increases (0.3 ppb yr^{-1}) in summertime O_3 at
5   Yellowstone National Park. While wildfire emissions can result in 2-8 ppb enhancements
6   to monthly mean O_3 at individual sites in some summers, they are not the primary driver
7   of observed O_3 interannual variability over the Intermountain West (**Figs.15 and 16**).
8   Instead, boundary layer depth, high temperatures and the associated buildup of O_3
9   produced from regional anthropogenic emissions contribute most to observed
10   year-to-year variability of O_3 in summer. We find that summertime O_3 measured in the
11   Denver Metropolitan area during pollution episodes frequently exceeds the 70 ppb
12   NAAQS level, with little overall trend despite stringent precursor emission controls
13   (**Fig.17c**), which likely reflects the influence from more frequent occurrences of hot
14   extremes in the last decade.
15   In contrast to the WUS, the observed trends of surface O_3 in the EUS are
16   overwhelmingly dominated by decreases in regional anthropogenic emissions. Following
17   the NO_x SIP Call, surface O_3 over the EUS manifested a downward shift in the
18   probability distribution, with the largest decreases occurring in the highest percentiles
19   during summer (-0.8 to -1.8 ppb yr^{-1}; **Fig.8**). Spatially, historical O_3 decreases during
20   non-summer seasons are most pronounced in the Southeast with an earlier onset of
21   biogenic isoprene emissions and NO_x-sensitive O_3 production (**Figs.7 and 9**). Regional
22   NO_x controls also alleviated the O_3 buildup during the recent heat waves of 2011 and
23   2012 relative to earlier heat waves (**Figs. 18 and 19**). Despite high mean state biases, the
24   model captures the salient features of observed O_3 trends over the EUS, including the
25   largest summertime decreases in the 95th percentile, the north-to-south gradient in
26   springtime O_3 trends, as well as wintertime increases in the 5th and 50th percentiles. The
27   model also captures enhancements in monthly mean O_3 due to large-scale heat waves.
28   Without anthropogenic emission controls, the 95th percentile summertime O_3 over the
29   EUS would have increased by 0.2-0.4 ppb yr^{-1} over 1988-2014 (**Fig.11c**), due to more
30   frequent hot summer extremes and increases in biogenic isoprene emissions over this
31   period **(Fig.12),** which may have offset some of air quality improvements gained from
32   regional NO_x reductions.
33

Atmospheric
Chemistry
and Physics
Discussions

Open Access

EGU

1 **References:**

2 Abatzoglou, J.T. and A.P. Williams (2016), Impact of anthropogenic climate change on
3 wildfire across western US forests, Proc. Natl. Acad. Sci. U.S.A., 11770–11775, doi:
4 10.1073/pnas.1607171113

6 Baker, K. R., M. C. Woody, G. S. Tonnesen, et al. (2016), Contribution of regional-scale
7 fire events to ozone and PM2.5 air quality estimated by photochemical modeling
8 approaches, Atmos. Environ., 140, 539-554, doi: 10.1016/j.atmosenv.2016.06.032.

10 Barnes, E. A., A. M. Fiore, and L. W. Horowitz (2016), Detection of trends in surface
11 ozone in the presence of climate variability, J. Geophys. Res., 121(10), 6112-6129, doi:
12 10.1002/2015jd024397.

13 Bishop, G. A., and D. H. Stedman (2008), A decade of on-road emissions measurements,
14 Environ. Sci. Technol., 42(5), 1651-1656, doi: 10.1021/es702413b.

15 Bishop, G. A., and D. H. Stedman (2015), Reactive Nitrogen Species Emission Trends in
16 Three Light-/Medium-Duty United States Fleets, Environ. Sci. Technol., 49(18),
17 11234-11240, doi: 10.1021/acs.est.5b02392.

18 Boersma, K. F., H. J. Eskes, and E. J. Brinksma (2004), Error analysis for tropospheric
19 NO_2 retrieval from space, J. Geophys. Res., 109(D4), doi: 10.1029/2003jd003962.

21 Brodin, M., D. Helmig, and S. Oltmans (2010), Seasonal ozone behavior along an
22 elevation gradient in the Colorado Front Range Mountains, Atmos. Environ., 44(39),
23 5305-5315, doi: 10.1016/j.atmosenv.2010.06.033.

24 Brown-Steiner, B., and P. Hess (2011), Asian influence on surface ozone in the United
25 States: A comparison of chemistry, seasonality, and transport mechanisms, J. Geophys.
26 Res., 116, doi: 10.1029/2011jd015846.

27 Brown-Steiner, B., P. G. Hess, and M. Y. Lin (2015), On the capabilities and limitations
28 of GCCM simulations of summertime regional air quality: A diagnostic analysis of ozone
29 and temperature simulations in the US using CESM CAM-Chem, Atmos. Environ., 101,
30 134-148, doi: 10.1016/j.atmosenv.2014.11.001.

31 Carmichael, G. R., et al. (2003), Regional-scale chemical transport modeling in support
32 of the analysis of observations obtained during the TRACE-P experiment, J. Geophys.
33 Res., 108(D21), doi: 10.1029/2002jd003117.

Atmospheric
Chemistry
and Physics
Discussions

Clifton, O. E., A. M. Fiore, G. Correa, L. W. Horowitz, and V. Naik (2014), Twenty-first century reversal of the surface ozone seasonal cycle over the northeastern United States, Geophys. Res. Lett., 41(20), 7343-7350, doi: 10.1002/2014gl061378.

Cooper, O. R., R.-S. Gao, D. Tarasick, T. Leblanc, and C. Sweeney (2012), Long-term ozone trends at rural ozone monitoring sites across the United States, 1990–2010, J. Geophys. Res., 117, doi: 10.1029/2012JD018261.

Cooper, O. R., et al. (2010), Increasing springtime ozone mixing ratios in the free troposphere over western North America, Nature, 463(7279), 344-348, doi: 10.1038/nature08708.

Dennison, P. E., S. C. Brewer, J. D. Arnold, and M. A. Moritz (2014), Large wildfire trends in the western United States, 1984-2011, Geophys. Res. Lett., 41(8), 2928-2933, doi: 10.1002/2014gl059576.

Dentener, F., et al. (2006), Emissions of primary aerosol and precursor gases in the years 2000 and 1750 prescribed data-sets for AeroCom, Atmos. Chem. Phys., 6, 4321-4344, 10.5194/acp-6-4321-2006

Ding, A. J., T. Wang, V. Thouret, J. P. Cammas, and P. Nedelec (2008), Tropospheric ozone climatology over Beijing: analysis of aircraft data from the MOZAIC program, Atmos. Chem. Phys., 8(1), 1-13, doi:10.5194/acp-8-1-2008

Donat, M. G., L. V. Alexander, H. Yang, I. Durre, R. Vose, and J. Caesar, 2013a: Global land-based datasets for monitoring climatic extremes. Bull. Amer. Meteor. Soc., 94, 997–1006, doi:10.1175/BAMS-D-12-00109.1.

Donner, L. J., et al. (2011), The Dynamical Core, Physical Parameterizations, and Basic Simulation Characteristics of the Atmospheric Component AM3 of the GFDL Global Coupled Model CM3, J. Clim., 24(13), 3484-3519, doi: 10.1175/2011jcli3955.1.

Duncan, B. N., L. N. Lamsal, A. M. Thompson et al. (2016), A space-based, high-resolution view of notable changes in urban NOx pollution around the world (2005-2014), J. Geophys. Res., 121(2), 976-996, doi: 10.1002/2015jd024121.

Emberson, L. D., N. Kitwiroon, S. Beevers, P. Buker, and S. Cinderby (2013), Scorched Earth: how will changes in the strength of the vegetation sink to ozone deposition affect human health and ecosystems?, Atmos. Chem. Phys., 13(14), 6741-6755, doi: 10.5194/acp-13-6741-2013.

Atmospheric
Chemistry
and Physics
Discussions

1 Federal Register (2015). US Environmental Protection Agency, National Ambient Air
2 Quality Standards for Ozone − Final Rule, Federal Register 80 (206), 65292-65468,
3 available at http://www.gpo.gov/fdsys/pkg/FR-2015-10-26/pdf/2015-26594.pdf.

4 Fiore, A. M., V. Naik, and E. M. Leibensperger (2015), Air Quality and Climate
5 Connections, J. Air Waste Manage. Assoc., 65(6), 645-685, doi:
6 10.1080/10962247.2015.1040526.

7 Fiore, A. M., J. T. Oberman, M. Y. Lin, L. Zhang, O. E. Clifton, D. J. Jacob, V. Naik, L.
8 W. Horowitz, and J. P. Pinto (2014), Estimating North American background ozone in
9 U.S. surface air with two independent global models: Variability, uncertainties, and
10 recommendations Atmos. Environ., 96, 284-300, doi:
11 doi:10.1016/j.atmosenv.2014.07.045.

12 Fiore, A. M., et al. (2009), Multimodel estimates of intercontinental source-receptor
13 relationships for ozone pollution, J. Geophys. Res., 114, doi: 10.1029/2008jd010816.

14 Gao, Y., J. S. Fu, J. B. Drake, J. F. Lamarque, and Y. Liu (2013), The impact of emission
15 and climate change on ozone in the United States under representative concentration
16 pathways (RCPs), Atmos. Chem. Phys., 13(18), 9607-9621, doi:
17 10.5194/acp-13-9607-2013.

18 Gilman, J. B., B. M. Lerner, W. C. Kuster, and J. A. de Gouw (2013), Source Signature of
19 Volatile Organic Compounds from Oil and Natural Gas Operations in Northeastern
20 Colorado, Environ. Sci. Technol., 47(3), 1297-1305, doi: 10.1021/es304119a.

21 Granier, C., et al. (2011), Evolution of anthropogenic and biomass burning emissions of
22 air pollutants at global and regional scales during the 1980-2010 period, Climatic Change,
23 109(1-2), 163-190, doi: 10.1007/s10584-011-0154-1.

24 Gratz, L. E., D. A. Jaffe, and J. R. Hee (2014), Causes of increasing ozone and decreasing
25 carbon monoxide in springtime at the Mt. Bachelor Observatory from 2004 to 2013,
26 Atmos. Environ., 109, 323-330, doi: 10.1016/j.atmosenv.2014.05.076.

27 Guenther, A., T. Karl, P. Harley, C. Wiedinmyer, P. I. Palmer, and C. Geron (2006),
28 Estimates of global terrestrial isoprene emissions using MEGAN (Model of Emissions of
29 Gases and Aerosols from Nature), Atmos. Chem. Phys., 6, 3181-3210.

30 Halliday, H. S., A. M. Thompson, and A. Wisthaler, et al. (2016), Atmospheric benzene
31 observations from oil and gas production in the Denver Julesburg basin in July and

1   August 2014, J. Geophys. Res. Atmos., 121, doi:10.1002/2016JD025327, 2016., 121, doi:
2   10.1002/2016JD025327.

3   Harris, I., P. D. Jones, T. J. Osborn, and D. H. Lister (2014), Updated high-resolution
4   grids of monthly climatic observations - the CRU TS3.10 Dataset, Journal of Climatology,
5   34(3), 623-642, doi: 10.1002/joc.3711.

6   Hilboll, A., A. Richter, and J. P. Burrows (2013), Long-term changes of tropospheric NO2
7   over megacities derived from multiple satellite instruments, Atmos. Chem. Phys., 13,
8   4145-4169, doi: 10.5194/acp-13-4145-2013.

9   Horton, D. E., N. C. Johnson, D. Singh, D. L. Swain, B. Rajaratnam, and N. S.
10 Diffenbaugh (2015), Contribution of changes in atmospheric circulation patterns to
11 extreme temperature trends, Nature, 522(7557), 465-469, doi: 10.1038/nature14550.

12 Huang, M., et al. (2013), Impacts of transported background pollutants on summertime
13 western US air quality: model evaluation, sensitivity analysis and data assimilation,
14 Atmos. Chem. Phys., 13(1), 359-391, doi: 10.5194/acp-13-359-2013.

15 Jacob, D. J., and D. A. Winner (2009), Effect of climate change on air quality, Atmos
16 Environ, 43(1), 51-63, doi: 10.1016/j.atmosenv.2008.09.051.

17 Jaffe, D. A., et al. (1999), Transport of Asian air pollution to North Amer- ica, Geophys.
18 Res. Lett., 26, 711–714, doi:10.1029/1999GL900100

19 Jaffe, D. (2011), Relationship between Surface and Free Tropospheric Ozone in the
20 Western U.S, Environ. Sci. Technol, 45(2), 432-438, doi: 10.1021/es1028102.

21 Jaffe, D., D. Chand, W. Hafner, A. Westerling, and D. Spracklen (2008), Influence of fires
22 on O3 concentrations in the western US, Environ. Sci. Technol., 42(16), 5885-5891, doi:
23 10.1021/es800084k.

24 Jaffe, D., N. Wigder, N. Downey, G. Pfister, A. Boynard, and S. B. Reid (2013), Impact
25 of Wildfires on Ozone Exceptional Events in the Western US, Environ. Sci. Technol.,
26 47(19), 11065-11072, doi: 10.1021/es402164f.

27 Jaffe, D., I. Bertschi, L. Jaegle, P. Novelli, J. S. Reid, H. Tanimoto, R. Vingarzan, and D.
28 L. Westphal (2004), Long-range transport of Siberian biomass burning emissions and
29 impact on surface ozone in western North America, Geophys. Res. Lett., 31(16), doi:

Atmospheric
Chemistry
and Physics
Discussions

1   10.1029/2004gl020093.

2   Jia, L. W., G. A. Vecchi, X. S. Yang, R. G. Gudgel, T. L. Delworth, W. F. Stern, K.
3   Paffendorf, S. D. Underwood, and F. R. Zeng (2016), The Roles of Radiative Forcing,
4   Sea Surface Temperatures, and Atmospheric and Land Initial Conditions in US Summer
5   Warming Episodes, J. Climate, 29(11), 4121-4135, doi: 10.1175/Jcli-D-15-0471.1.

6   John, J. G., A. M. Fiore, V. Naik, L. W. Horowitz, and J. P. Dunne (2012), Climate versus
7   emission drivers of methane lifetime against loss by tropospheric OH from 1860-2100,
8   Atmos. Chem. Phys., 12(24), 12021-12036, doi: 10.5194/acp-12-12021-2012.

9   Koumoutsaris, S., and I. Bey (2012), Can a global model reproduce observed trends in
10   summertime surface ozone levels?, Atmos. Chem. Phys., 12(15), 6983-6998, doi:
11   10.5194/acp-12-6983-2012.

12   Lamarque, J. F., G. P. Kyle, M. Meinshausen, K. Riahi, S. J. Smith, D. P. van Vuuren, A. J.
13   Conley, and F. Vitt (2012), Global and regional evolution of short-lived radiatively-active
14   gases and aerosols in the Representative Concentration Pathways, Climatic Change
15   109(1-2), 191-212, doi: 10.1007/s10584-011-0155-0.

16   Lamarque, J. F., et al. (2010), Historical (1850-2000) gridded anthropogenic and biomass
17   burning emissions of reactive gases and aerosols: methodology and application, Atmos.
18   Chem. Phys., 10(15), 7017-7039, doi: 10.5194/acp-10-7017-2010.

19   Langford, A. O., K. C. Aikin, C. S. Eubank, and E. J. Williams (2009), Stratospheric
20   contribution to high surface ozone in Colorado during springtime, Geophys. Res. Lett., 36,
21   doi: 10.1029/2009gl038367.

22   Langford, A. O., C. J. Senff, R. J. Alvarez, II, R. M. Banta, and R. M. Hardesty (2010),
23   Long-range transport of ozone from the Los Angeles Basin: A case study, Geophys. Res.
24   Lett., 37, doi: 10.1029/2010gl042507.

25   Langford, A. O., et al. (2014), An overview of the 2013 Las Vegas Ozone Study (LVOS):
26   Impact of stratospheric intrusions and long-range transport on surface air quality, Atmos.
27   Environ., 109, 305-322, doi: 10.1016/j.atmosenv.2014.08.040.

28   Lee, H.-J., S.-W. Kim, J. Brioude, O. R. Cooper, G. J. Frost, C.-H. Kim, R. J. Park, M.
29   Trainer, and J.-H. Woo (2014), Transport of NOx in East Asia identified by satellite and in
30   situ measurements and Lagrangian particle dispersion model simulations, , J. Geophys.
31   Res. Atmos., 119, 2574-2596, doi: doi:10.1002/ 2013JD021185.

Atmospheric
Chemistry
and Physics
Discussions

1   Leibensperger, E. M., L. J. Mickley, and D. J. Jacob (2008), Sensitivity of US air quality
2   to mid-latitude cyclone frequency and implications of 1980-2006 climate change, Atmos.
3   Chem. Phys., 8(23), 7075-7086.

4   Li, G., Bei, N., Cao, J., Wu, J., Long, X., Feng, T., Dai, W., Liu, S., Zhang, Q., and Tie,
5   X.: Widespread and Persistent Ozone Pollution in Eastern China, Atmos. Chem. Phys.
6   Discuss., doi:10.5194/acp-2016-864, in review, 2016.

7   Lin, M. Y., T. Holloway, G. R. Carmichael, and A. M. Fiore (2010), Quantifying pollution
8   inflow and outflow over East Asia in spring with regional and global models, Atmos.
9   Chem. Phys., 10(9), 4221-4239, doi: 10.5194/acp-10-4221-2010.

10 Lin, M. Y., T. Holloway, T. Oki, D. G. Streets, and A. Richter (2009), Multi-scale model
11 analysis of boundary layer ozone over East Asia, Atmos. Chem. Phys., 9(10), 3277-3301,
12 doi: 10.5194/acp-9-3277-2009.

13 Lin, M. Y., L. W. Horowitz, S. J. Oltmans, A. M. Fiore, and S. Fan (2014), Tropospheric
14 ozone trends at Mauna Loa Observatory tied to decadal climate variability, Nature
15 Geoscience, 7, 136–143, doi: 10.1038/ngeo2066.

16 Lin, M. Y., A. M. Fiore, L. W. Horowitz, A. O. Langford, S. J. Oltmans, D. Tarasick, and
17 H. E. Rieder (2015a), Climate variability modulates western U.S. ozone air quality in
18 spring via deep stratospheric intrusions, Nature Communications, 6(7105), doi:
19 10.1038/ncomms8105.

20 Lin, M. Y., A. M. Fiore, O. R. Cooper, L. W. Horowitz, A. O. Langford, H. Levy, B. J.
21 Johnson, V. Naik, S. J. Oltmans, and C. J. Senff (2012a), Springtime high surface ozone
22 events over the western United States: Quantifying the role of stratospheric intrusions, J.
23 Geophys. Res., 117, D00V22, doi: 10.1029/2012jd018151.

24 Lin, M. Y., L. W. Horowitz, O. R. Cooper, D. Tarasick, S. Conley, L. T. Iraci, B. Johnson,
25 T. Leblanc, I. Petropavlovskikh, and E. L. Yates (2015b), Revisiting the evidence of
26 increasing springtime ozone mixing ratios in the free troposphere over western North
27 America, Geophys. Res. Lett., 42(20), 8719-8728, doi: 10.1002/2015GL065311.

28 Lin, M. Y., et al. (2012b), Transport of Asian ozone pollution into surface air over the
29 western United States in spring, J. Geophys. Res., 117, D00V07, doi:
30 10.1029/2011jd016961.

31 Lin, Y.-K., T.-H. Lin, and S.-C. Chang (2010), The changes in different ozone metrics and

Atmospheric
Chemistry
and Physics
Discussions

Open Access

1 their implications following precursor reductions over northern Taiwan from 1994 to
2 2007, Environ. Monit. Assess., 169(1-4), 143-157, doi: 10.1007/s10661-009-1158-4.

3 Liu, H. Y., D. J. Jacob, L. Y. Chan, S. J. Oltmans, I. Bey, R. M. Yantosca, J. M. Harris, B.
4 N. Duncan, and R. V. Martin (2002), Sources of tropospheric ozone along the Asian
5 Pacific Rim: An analysis of ozonesonde observations, J. Geophys. Res., 107(D21), doi:
6 4573 10.1029/2001jd002005.

7 Loughner, C. P., B. N. Duncan, and J. Hains (2014), The benefit of historical air pollution
8 emissions reductions during extreme heat, Environmental Manager (September), 34-38.

9   Ma, Z., J. Xu, W. Quan, Z. Zhang, W. Lin, and X. Xu (2016), Significant increase of
10 surface ozone at a rural site, north of eastern China, Atmos. Chem. Phys., 16, 3969-3977,
11 doi: doi:10.5194/acp-16-3969-2016.

12 McDonald, B. C., T. R. Dallmann, E. W. Martin, and R. A. Harley (2012), Long-term
13 trends in nitrogen oxide emissions from motor vehicles at national, state, and air basin
14 scales, J. Geophys. Res., 117, D00V18, doi: 10.1029/2012jd018304.

15 McDuffie, E. E., et al. (2016), Influence of oil and gas emissions on summertime ozone
16 in the Colorado Northern Front Range, J. Geophys. Res. Atmos., 121, doi:
17 10.1002/2016JD025265.

18 Monks, P. S., Archibald, A. T., Colette, A., et al. (2015): Tropospheric ozone and its
19 precursors from the urban to the global scale from air quality to short-lived climate forcer,
20 Atmos. Chem. Phys., 15, 8889-8973, doi:10.5194/acp-15-8889-2015.

21 Parrish, D. D., et al. (2014), Long-term changes in lower tropospheric baseline ozone
22 concentrations: Comparing chemistry-climate models and observations at northern
23 midlatitudes, J. Geophys. Res., 119(9), 5719-5736, doi: 10.1002/2013JD021435.

24 Pfister, G. G., C. Wiedinmyer, and L. K. Emmons (2008), Impacts of the fall 2007
25 California wildfires on surface ozone: Integrating local observations with global model
26 simulations, Geophys. Res. Lett., 35(19), doi: 10.1029/2008gl034747.

27 Pfister, G. G., S. Walters, L. K. Emmons, D. P. Edwards, and J. Avise (2013), Quantifying
28 the contribution of inflow on surface ozone over California during summer 2008, J.
29 Geophys. Res., 118(21), 12282-12299, doi: 10.1002/2013jd020336.

Atmospheric
Chemistry
and Physics
Discussions

1 Pfister, G. G., S. Walters, J. F. Lamarque, J. Fast, M. C. Barth, J. Wong, J. Done, G.
2 Holland, and C. L. Bruyere (2014), Projections of future summertime ozone over the US,
3 J. Geophys. Res., 119(9), 5559-5582, doi: 10.1002/2013jd020932.

4 Porter, W. C., C. L. Heald, D. Cooley, and B. Russell (2015), Investigating the observed
5 sensitivities of air-quality extremes to meteorological drivers via quantile regression,
6 Atmos. Chem. Phys., 15(18), 10349-10366, doi: 10.5194/acp-15-10349-2015.

7 Pusede, S. E., A. L. Steiner, and R. C. Cohen (2015), Temperature and Recent Trends in
8 the Chemistry of Continental Surface Ozone, Chem. Rev., 115(10), 3898-3918, doi:
9 10.1021/cr5006815.

10 Rasmussen, D. J., A. M. Fiore, V. Naik, L. W. Horowitz, S. J. McGinnis, and M. G.
11 Schultz (2012), Surface ozone-temperature relationships in the eastern US: A monthly
12 climatology for evaluating chemistry-climate models, Atmos. Environ., 47, 142-153, doi:
13 10.1016/j.atmosenv.2011.11.021.

14 Reidmiller, D. R., et al. (2009), The influence of foreign vs. North American emissions on
15 surface ozone in the US, Atmos. Chem. Phys., 9(14), 5027-5042,
16 doi:10.5194/acp-9-5027-2009

17 Rieder, H. E., A. M. Fiore, L. W. Horowitz, and V. Naik (2015), Projecting
18 policy-relevant metrics for high summertime ozone pollution events over the eastern
19 United States due to climate and emission changes during the 21st century, J. Geophys.
20 Res., 120(2), 784-800, doi: 10.1002/2014jd022303.

21 Russell, A. R., L. C. Valin, and R. C. Cohen (2012), Trends in OMI NO2 observations
22 over the United States: effects of emission control technology and the economic recession,
23 Atmos. Chem. Phys., 12(24), 12197-12209, doi: 10.5194/acp-12-12197-2012.

24 Schnell, J. L., M. J. Prather, B. Josse, V. Naik, L. W. Horowitz, G. Zeng, D. T. Shindell,
25 and G. Faluvegi (2016), Effect of climate change on surface ozone over North America,
26 Europe, and East Asia, Geophys. Res. Lett., 43, 3509-3518, doi: 10.1002/2016GL068060.

27 Schultz, M. G., A. Heil, J. J. Hoelzemann, A. Spessa, K. Thonicke, J. G. Goldammer, A.
28 C. Held, J. M. C. Pereira, and M. van het Bolscher (2008), Global wildland fire emissions
29 from 1960 to 2000, Global Biogeochem. Cycles, 22(2), doi: 10.1029/2007gb003031.

30 Schwietzke, S., et al. (2016), Upward revision of global fossil fuel methane emissions
31 based on isotope database, Nature, 538(7623), 88-91, doi: 10.1038/nature19797.

Atmospheric
Chemistry
and Physics
Discussions

1 Seager, R., and M. Hoerling (2014), Atmosphere and Ocean Origins of North American
2 Droughts, J. Climate, 27(12), 4581-4606, doi: 10.1175/Jcli-D-13-00329.1.

3 Shen, L., L. J. Mickley, and E. Gilleland (2016), Impact of increasing heat waves on US
4 ozone episodes in the 2050s: Results from a multimodel analysis using extreme value
5 theory, Geophys. Res. Lett., 43(8), 4017-4025, doi: 10.1002/2016gl068432.
6

7 Shepherd, T. G. (2015), CLIMATE SCIENCE: The dynamics of temperature extremes,
8 Nature, 522(7557), 422-424.

9   Simon, H., A. Reff, B. Wells, J. Xing, and N. Frank (2015), Ozone Trends Across the
10 United States over a Period of Decreasing NOx and VOC Emissions, Environ. Sci.
11 Technol., 49(1), 186-195, doi: 10.1021/es504514z.

12 Solberg, S., O. Hov, A. Sovde, I. S. A. Isaksen, P. Coddeville, H. De Backer, C. Forster, Y.
13 Orsolini, and K. Uhse (2008), European surface ozone in the extreme summer 2003, J.
14 Geophys. Res., 113(D7), doi:10.1029/2007jd009098.

15 Strode, S. A., J. M.Rodriguez, J.A. Logan, et al. (2015), Trends and variability in surface
16 ozone over the United States, J. Geophys. Res., 120, 9020 -9042, doi: 10.1002/
17 2014JD022784.

18 Sun, L., L. Xue, T. Wang, J. Guo, A. Ding, O.R. Cooper and M.Y. Lin, et al. (2016),
19 Significant increase of summertime ozone at Mount Tai in Central Eastern China, Atmos.
20 Chem. Phys., 16, 10637-10650, doi: 10.5194/acp-16-10637-2016.

21 Tanimoto, H. (2009), Increase in springtime tropospheric ozone at a mountainous site in
22 Japan for the period 1998-2006, Atmos. Environ., 43(6), 1358-1363, doi:
23 10.1016/j.atmosenv.2008.12.006.

24 Tanimoto, H., R. M. Zbinden, V. Thouret, and P. Nedelec (2016), Consistency of
25 tropospheric ozone observations made by different platforms and techniques in the global
26 databases. , Tellus Series B-Chemical and Physical Meteorology, 67, 27073, doi:
27 10.3402/tellusb.v67.27073.

28 Thompson, A.M., J.C. Witte, H.G.J. Smit, S.J. Oltmans, B.J. Johnson, V.W.J H. Kirchhoff,
29 and F.J. Schmidlin (2007), Southern Hemisphere Additional Ozonesondes (SHADOZ)
30 1998-2004 tropical ozone climatology: 3. Instrumentation, station-to-station variability,
31 and evaluation with simulated flight profiles, J. Geophys. Res., 112, D03304,

Atmospheric
Chemistry
and Physics
Discussions

1   doi:10.1029/2005JD007042.

2   Travis, K. R., et al. (2016), Why do models overestimate surface ozone in the Southeast
3   United States?, Atmos. Chem. Phys., 16, 13561-13577, doi: 10.5194/acp-16-13561-2016.

5   van der Werf, G. R., J. T. Randerson, L. Giglio, G. J. Collatz, M. Mu, P. S. Kasibhatla, D.
6   C. Morton, R. S. DeFries, Y. Jin, and T. T. van Leeuwen (2010), Global fire emissions and
7   the contribution of deforestation, savanna, forest, agricultural, and peat fires (1997-2009),
8   Atmos. Chem. Phys., 10(23), 11707-11735, doi: 10.5194/acp-10-11707-2010.

9   Wang, T., A. Ding, J. Gao, and W. S. Wu (2006), Strong ozone production in urban
10   plumes   from   Beijing,   China,   Geophys.   Res.   Lett.,   33,   L21806,
11   doi:10.1029/2006GL027689.

12   Wang, T., X. L. Wei, A. J. Ding, C. N. Poon, K. S. Lam, Y. S. Li, L. Y. Chan, and M.
13   Anson (2009), Increasing surface ozone concentrations in the background atmosphere of
14   Southern   China,   1994-2007,   Atmos.   Chem.   Phys.,   9,   6217-6227,   doi:
15   doi:10.5194/acp-9-6217-2009.

16   Wang, Y., Y. Xie, L. Cai, W. Dong, Q. Zhang, and L. Zhang (2015), Impact of the 2011
17   Southern US Drought on Ground-Level Fine Aerosol Concentration in Summertime, J.
18   Atmos. Sci., 72(3), 1075-1093, doi: 10.1175/jas-d-14-0197.1.

19   Wang, Y., McElroy, M. B., Munger, J. W., Hao, J., Ma, H., Nielsen, C. P., and Chen, Y.
20   (2008): Variations of O_3 and CO in summertime at a rural site near Beijing, Atmos. Chem.
21   Phys., 8(21), 6355–6363.

22   Warneke, C., J. A. de Gouw, J. S. Holloway, J. Peischl, T. B. Ryerson, E. Atlas, D. Blake,
23   M. Trainer, and D. D. Parrish (2012), Multiyear trends in volatile organic compounds in
24   Los Angeles, California: Five decades of decreasing emissions, J. Geophys. Res., 117, doi:
25   10.1029/2012jd017899.

26   Xu, W., W. Lin, X. Xu, J. Tang, J. Huang, H. Wu, and X. Zhang (2016), Long-term trends
27   of surface ozone and its influencing factors at the Mt Waliguan GAW station, China - Part
28   1: Overall trends and characteristics, Atmos. Chem. Phys., 16, 6191-6205, doi:
29   doi:10.5194/acp-16-6191-2016.

30   Yang, J., H. Q. Tian, B. Tao, W. Ren, S. F. Pan, Y. Q. Liu, and Y. H. Wang (2015), A
31   growing importance of large fires in conterminous United States during 1984-2012, J
32   Geophys Res-Biogeo, 120(12), 2625-2640, doi: 10.1002/2015jg002965.

Atmospheric
Chemistry
and Physics
Discussions

Open Access

1 Yurganov, L. N., et al. (2005), Increased Northern Hemispheric carbon monoxide burden
2 in the troposphere in 2002 and 2003 detected from the ground and from space, Atmos.
3 Chem. Phys., 5, 563-573.

4 Zhang, L., et al. (2008), Transpacific transport of ozone pollution and the effect of recent
5 Asian emission increases on air quality in North America: an integrated analysis using
6 satellite, aircraft, ozonesonde, and surface observations, Atmos. Chem. Phys., 8(20),
7 6117-6136, doi: 10.5194/acp-8-6117-2008.
8
9 Zhang, L., D. J. Jacob, X. Yue, N. V. Downey, D. A. Wood, and D. Blewitt (2014),
10 Sources contributing to background surface ozone in the US Intermountain West, Atmos.
11 Chem. Phys., 14(11), 5295-5309, doi: 10.5194/acp-14-5295-2014.

12 Zhang, Y., O. R. Cooper, A. Gaudel, A. M. Thompson, Philippe Nédélec, S.-Y. Ogino,
13 and J. J. West, Tropospheric ozone change from 1980 to 2010 dominated by equatorward
14 redistribution of emissions, Nature Geoscience, doi:10.1038/ngeo2827, 2016.
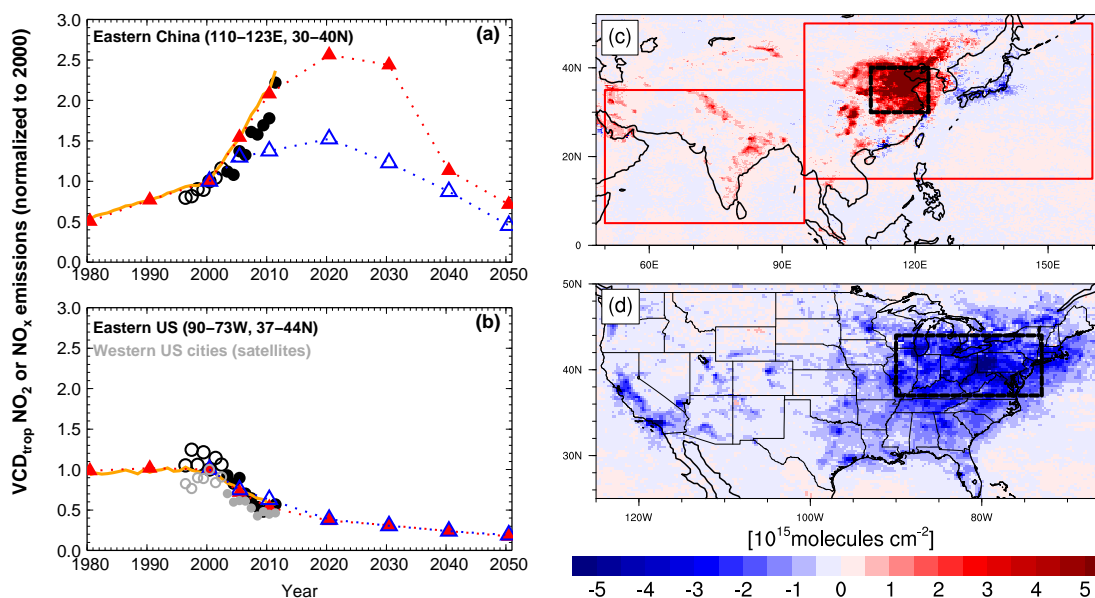
Figure 1. **Changes in NO_x emissions**. (a-b) Mean annual vertical column densities of tropospheric (VCD_{trop}) NO_2 normalized to year 2000 for the Eastern China and Eastern US domains (black boxes on map) from GOME (1996-2002, open circles) and SCIAMACHY (2003-2011, closed circles) measurements and AM3_BASE simulations (orange lines). Triangles indicate trends in NO_x emissions (normalized to 2000) from Lamarque et al. (2010) with annual interpolation after 2000 to RCP8.5 (red) versus RCP4.5 (blue). (c-d) Differences in annual mean SCIAMACHY VCD_{trop} NO_2 from 2003-2005 to 2009-2011. The red boxes denote the regions where emissions vary over time in the IAVASIA simulation (Table 1). Satellite NO_2 data are from www.temis.nl, with retrieval technique described in Boersma et al.(2004).

Atmospheric
Chemistry
and Physics
Discussions

Open Access
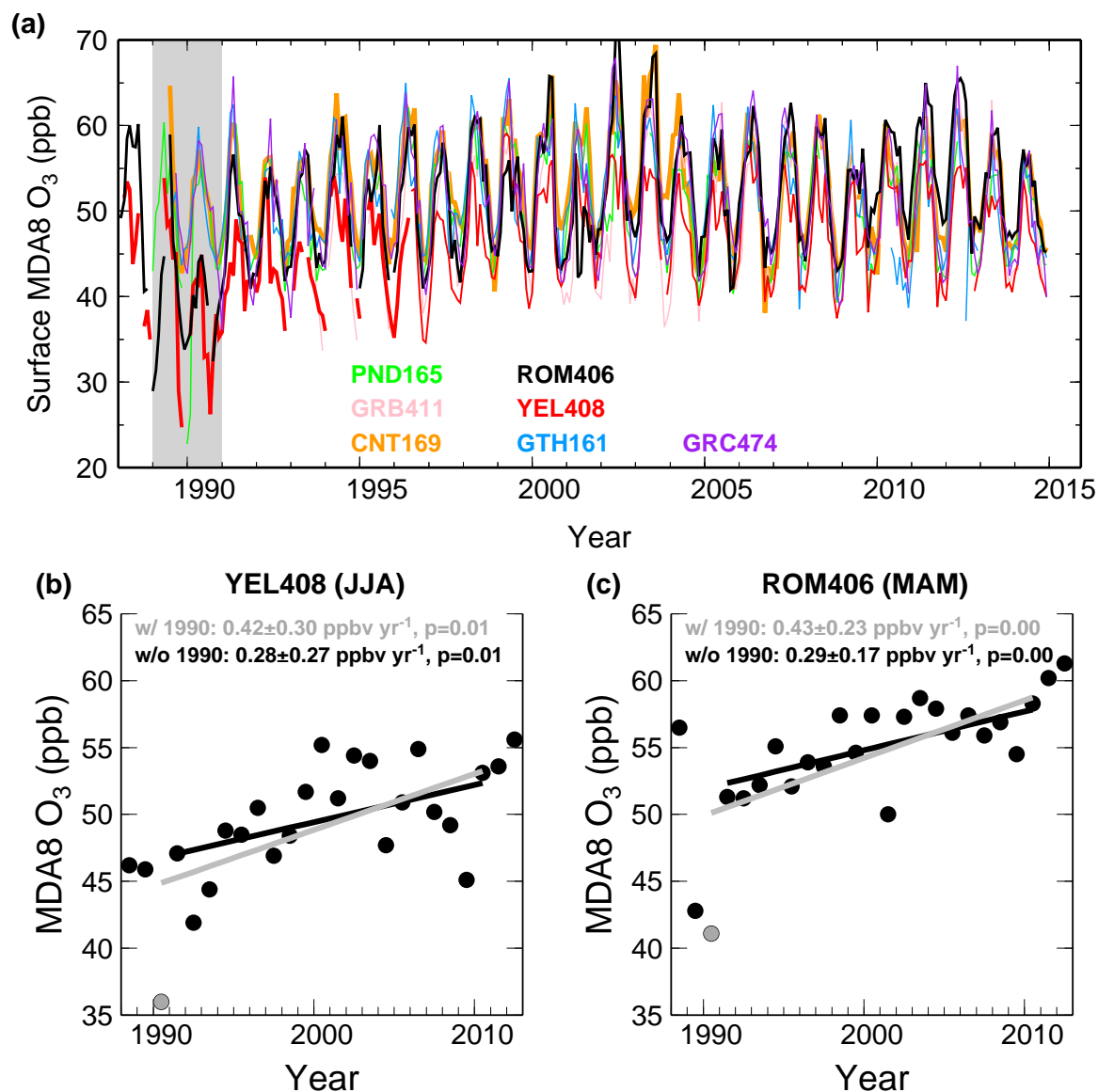
Figure 2. **Measurement uncertainties**. (a) Comparison of observed monthly mean MDA8 O_3 at WUS CASTNet sites. All sites have more than 90% data availability in every month shown. The grey shading denotes the period when data at Yellowstone (red) and Rocky Mountain (black) were inconsistent with the other sites. (b-c) The 1990-2010 trends of median JJA MDA8 O_3 at Yellowstone and median MAM MDA8 O_3 at Rocky Mountain with and without data in 1990.
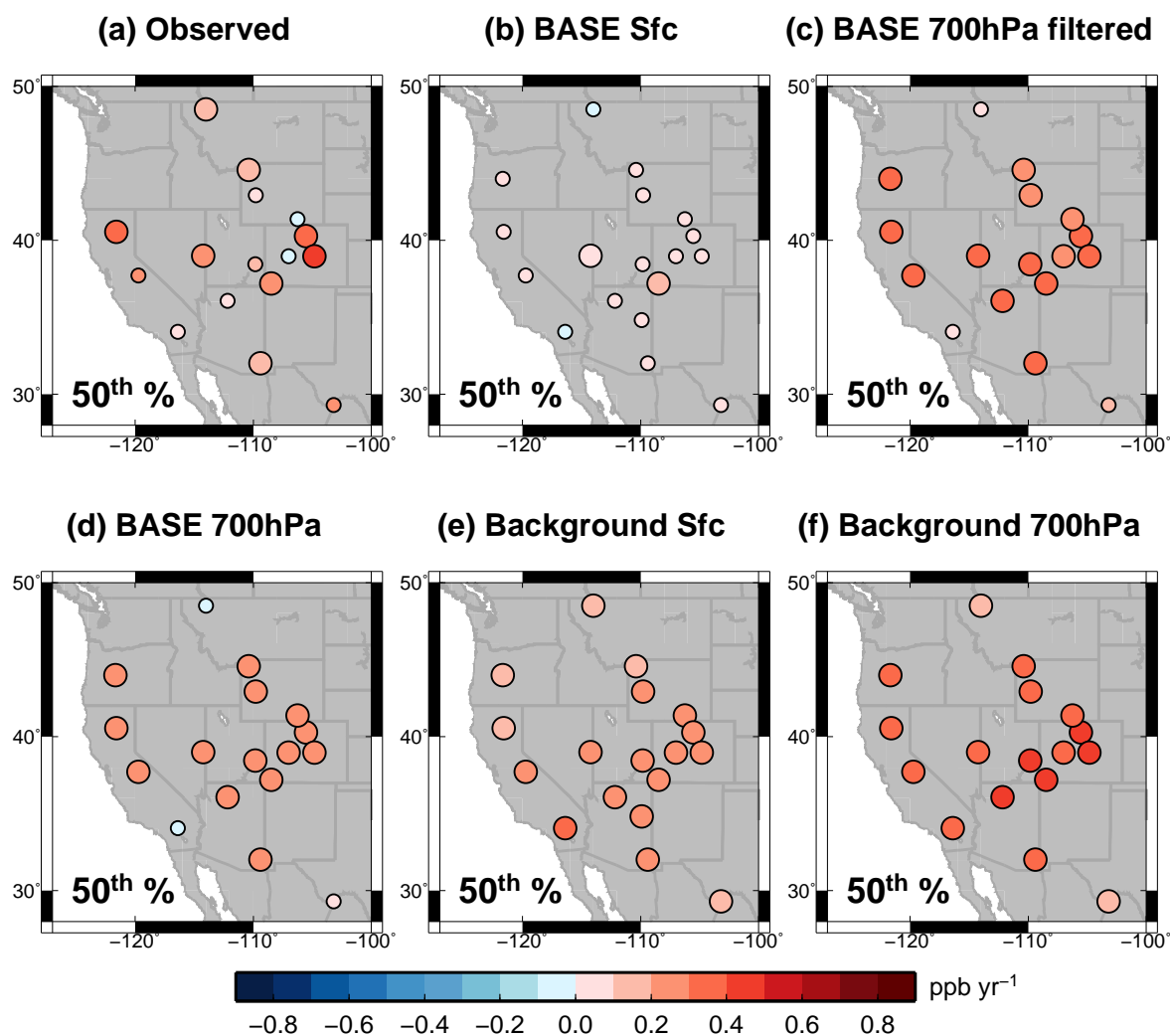
Figure 3. **Influence of baseline sampling.** Median spring MDA8 O$_3$ trends over 1988-2014 at WUS sites from: (a) Observations; (b) BASE model sampled at the surface; (c) BASE sampled at 700 hPa and filtered to remove the influence from fresh local pollution (see Sect. 2.4); (d) BASE sampled at 700 hPa without filtering; and (e-f) Background (with North American anthropogenic emissions shut off) sampled at the surface versus at 700 hPa. Note that three low-elevation (<1.5 km) sites Joshua Tree, Big Bend and Glacier National Parks are always sampled at the surface. Larger circles indicate sites with statistically signficant trends (p<0.05).

Atmospheric
Chemistry
and Physics
Discussions
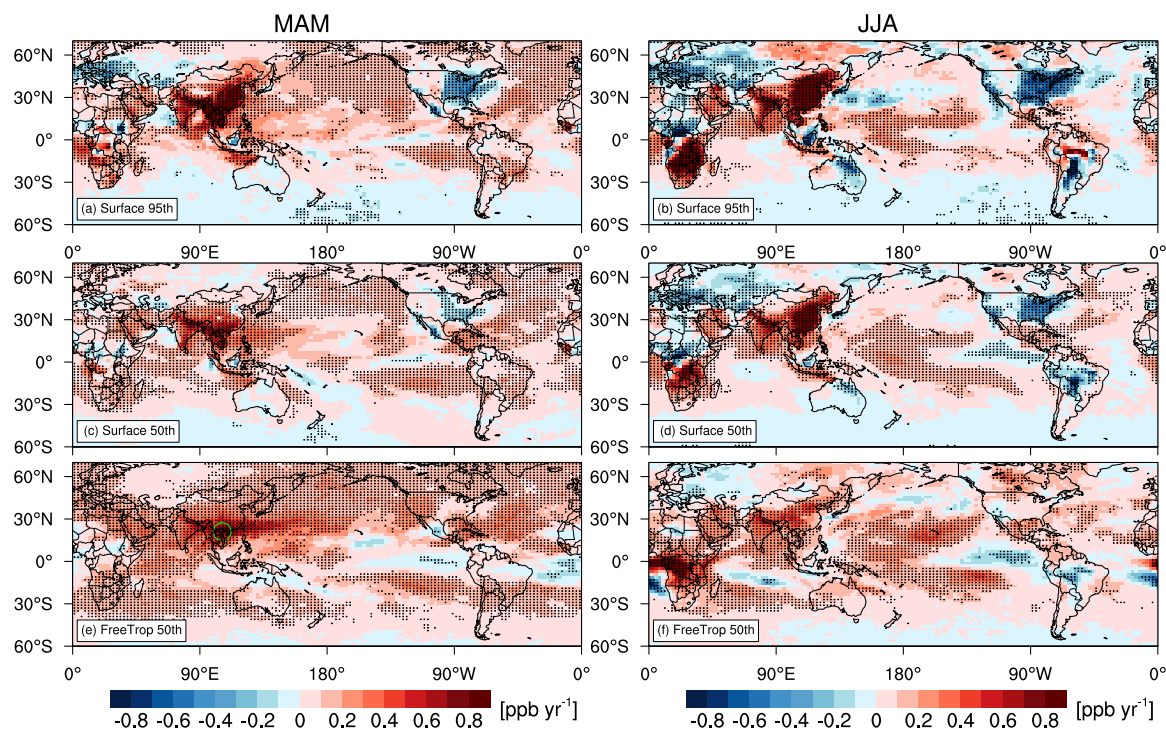
Figure 4. Global distribution of MDA8 O$_3$ trends from AM3_BASE over 1988-2014 for boreal spring (left) and summer (right) for the 95th percentile at the surface (a-b), median at the surface (c-d), and median in the free troposphere (700 hPa; e-f). Stippling indicates areas where the trend is statistically significant (p<0.05). The color scale is designed to resolve regional features rather than extreme values and saturates. The range of trends is -1 to +2.5 ppb yr^{-1}.

Atmospheric
Chemistry
and Physics
Discussions
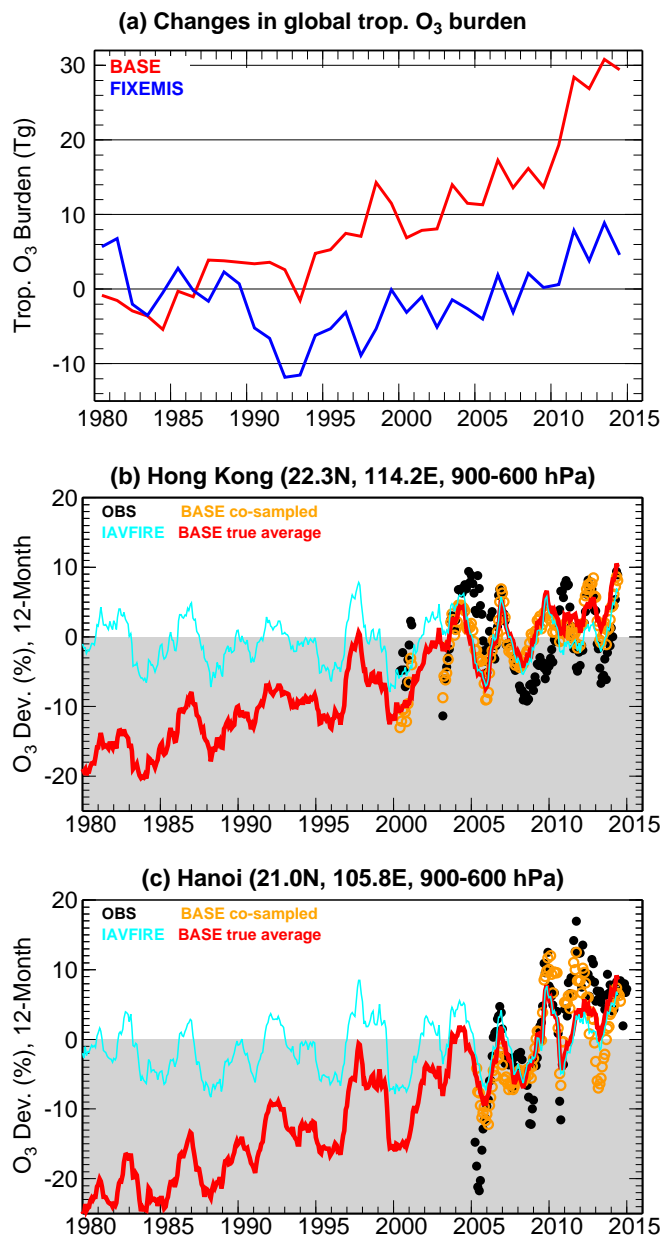
Figure 5. **(a)** Time series of changes in global tropospheric O_3 burden relative to the 1981-1990 mean from BASE and FIXEMIS simulations (Table 1). **(b)** Time series of 12-month running mean anomalies (in percent relative to the 2005-2014 mean) of O_3 averaged over 900-600 hPa at Hong Kong from: the averages of ozonesonde samples (black circles) and BASE model co-sampled on sonde launch days (orange circles) versus the true average from BASE and IAVFIRE with continuous daily sampling (solid lines). **(c)** Same as **(b)** but for Hanoi.
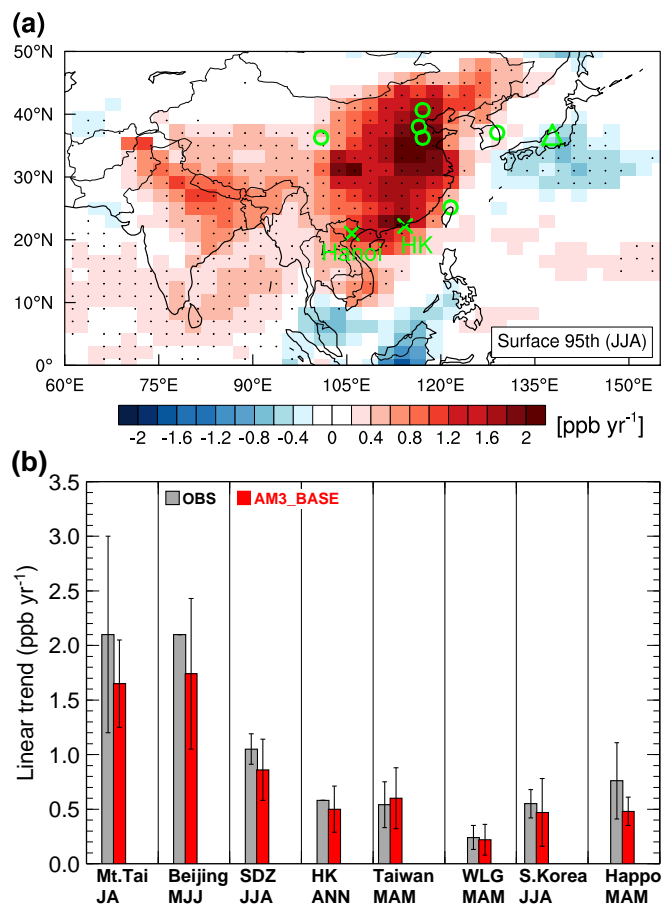
Figure 6. **Surface O$_3$ trends in Asia.** (a) Observation sites superimposed on a map of the 95th percentile summer MDA8 O$_3$ trends over 1995-2014 from AM3_BASE. (b) Comparison of median O$_3$ trends from AM3 (1995-2014) with observations (see text for periods): in Central Eastern China at Mt. Tai (July-August, Sun et al. 2016), Beijing (May-June-July, Ding et al. 2008) and Shangdianzi (SDZ) (JJA, Ma et al. 2016); in South China at Hong Kong (HK) (annual average, Wang et al. 2009) and Taiwan (MAM, Lin YK et al. 2010); at Mt. Waliguan (WLG) in western China (MAM, Xu et al. 2016); at South Korea (JJA, Lee et al. 2013) and Mt. Happo Japan (MAM, Tanimoto 2009). For Mt. Happo (triangle on map) AM3 is sampled at 700 hPa and filtered for the influence from Asian continental air - more representative of observed baseline conditions.
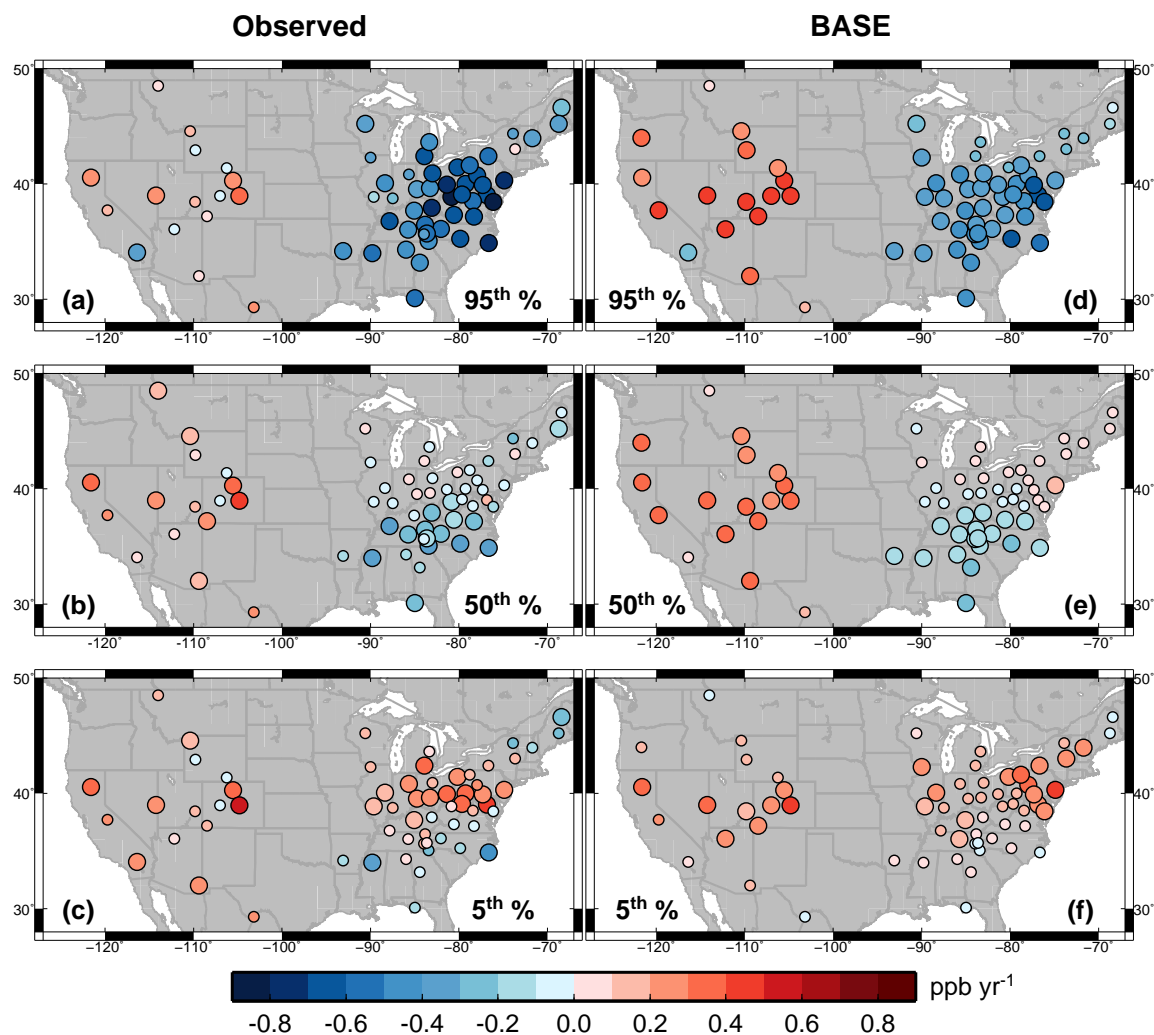
Figure 7. Linear trends in spring (MAM) MDA8 O_3 over 1988-2014 at US rural sites for the 95th, 50th, and 5th percentiles as observed (left) and simulated (right) in AM3 BASE. Larger circles indicate sites with statistically significant trends ($p < 0.05$). For WUS high-elevation sites, the model is sampled at 700 hPa and filtered to remove local influence (see text in Sect. 2.4).
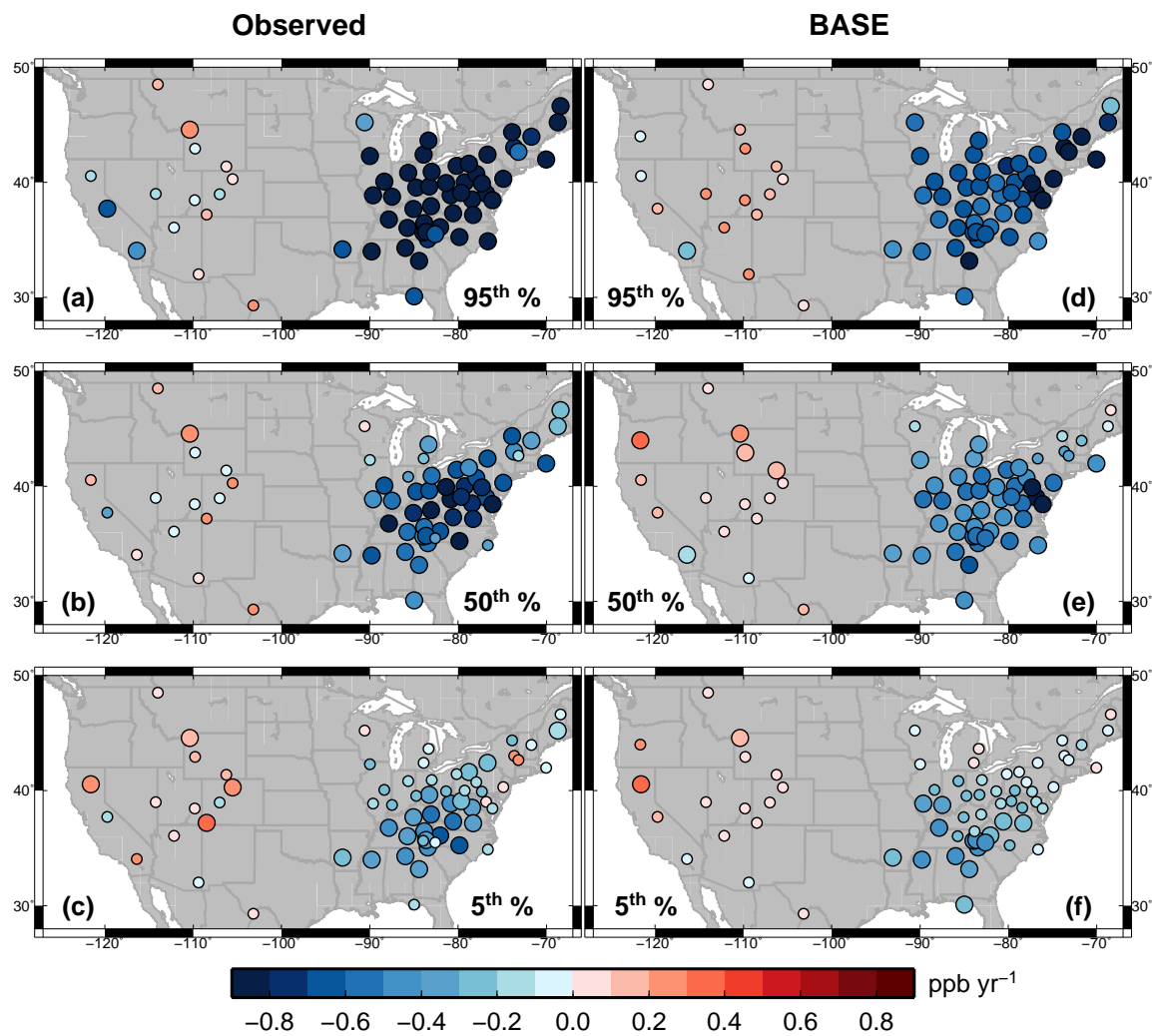
Figure 8. As in Figure 7, but for summer (JJA). Note that the colorbar saturates at -0.8.
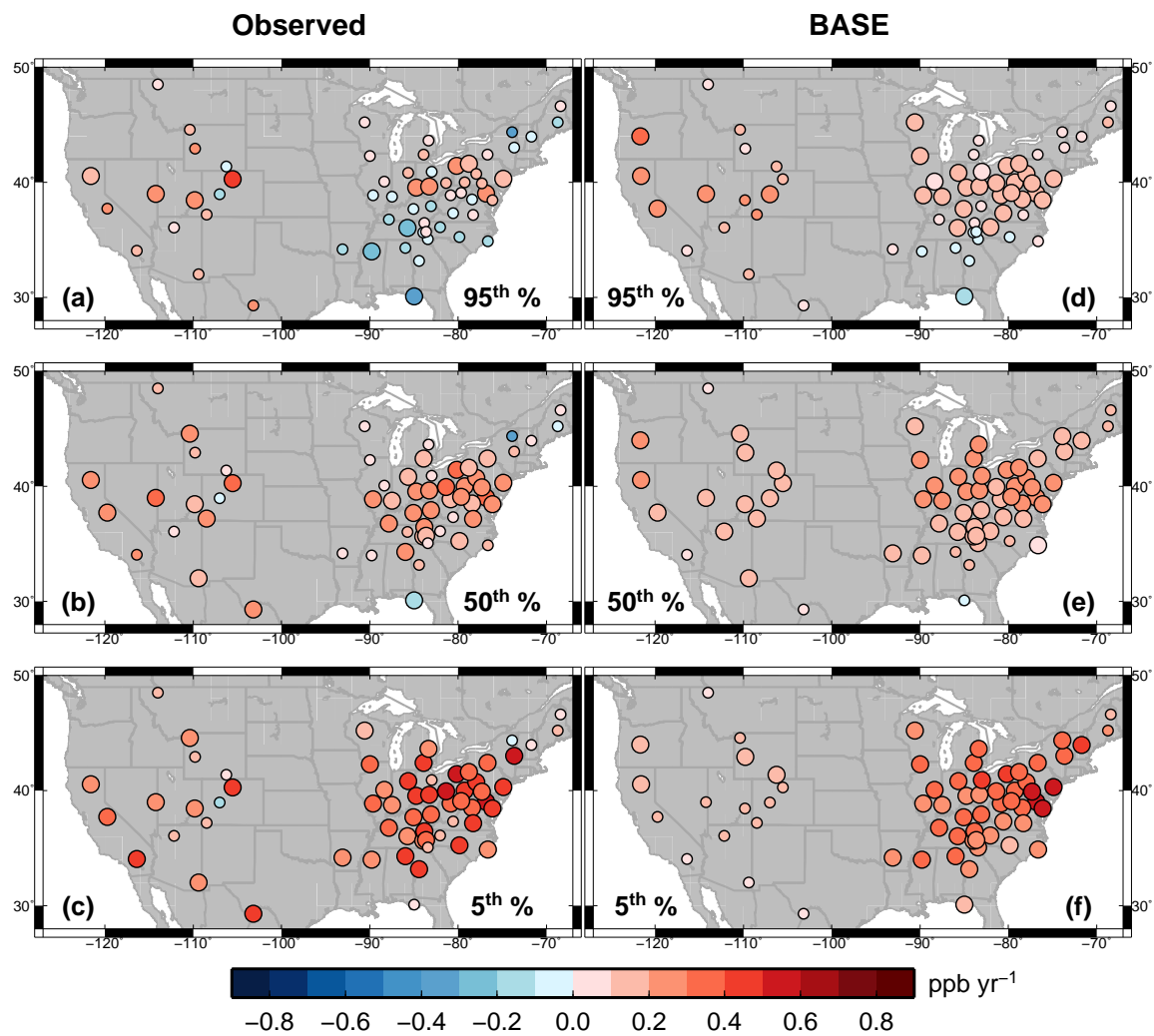
Figure 9. As in Figure 7, but for winter (DJF).
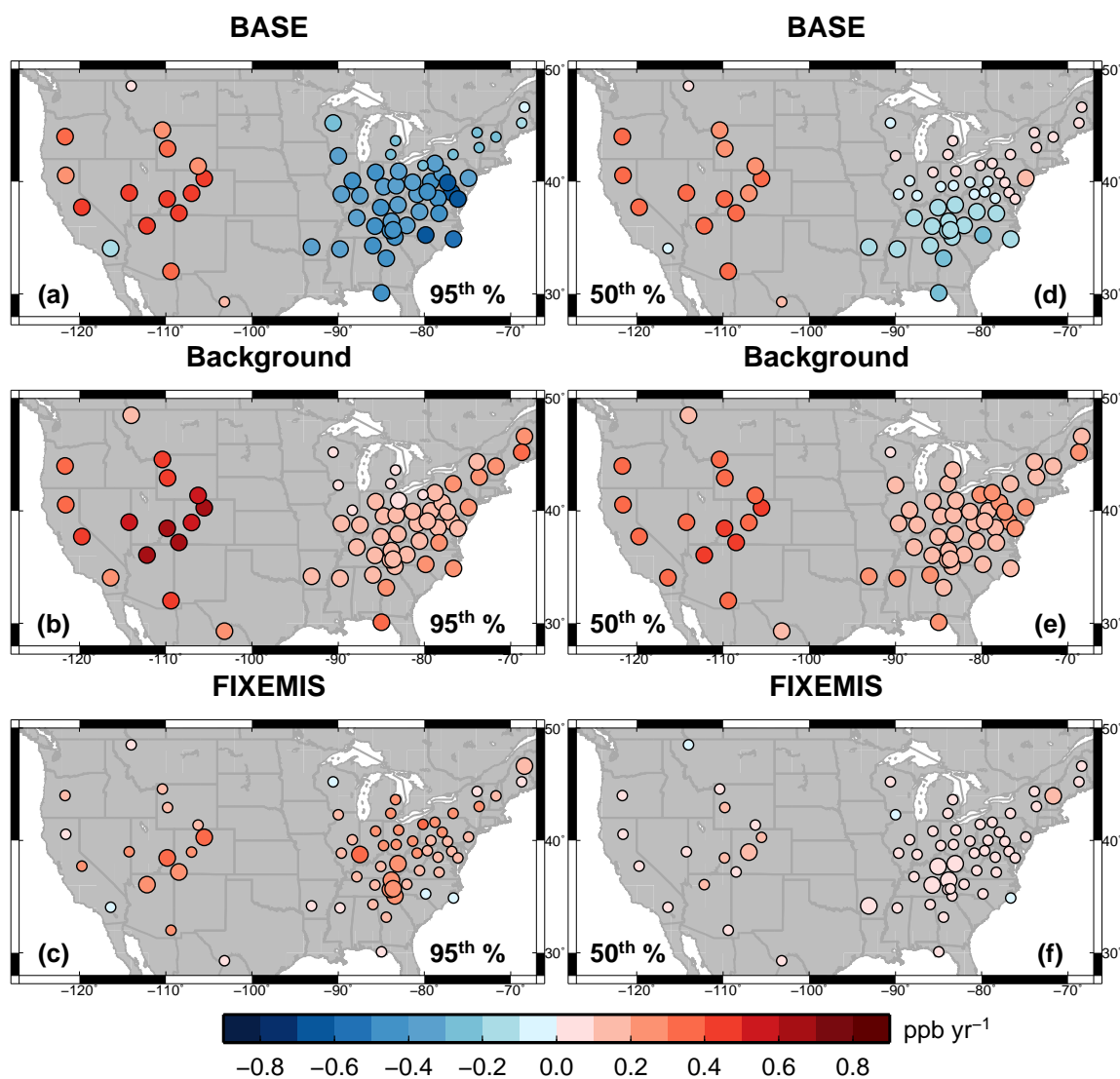
Figure 10. Linear trends in the 95th (left) and 50th (right) percentile springtime MDA8 O_3 over 1988-2014 at US rural sites from BASE (top), Background (middle) and FIXEMIS simulations (bottom). Larger circles indicate sites with statistically significant trends ($p<0.05$). Top panels are repeated from Fig.7d,e. Note that the 95th (50th) percentile is sampled seperately from the Background and FIXEMIS simulations without depending on the times when the BASE simulation is experiencing the 95th (50th) percentile days.
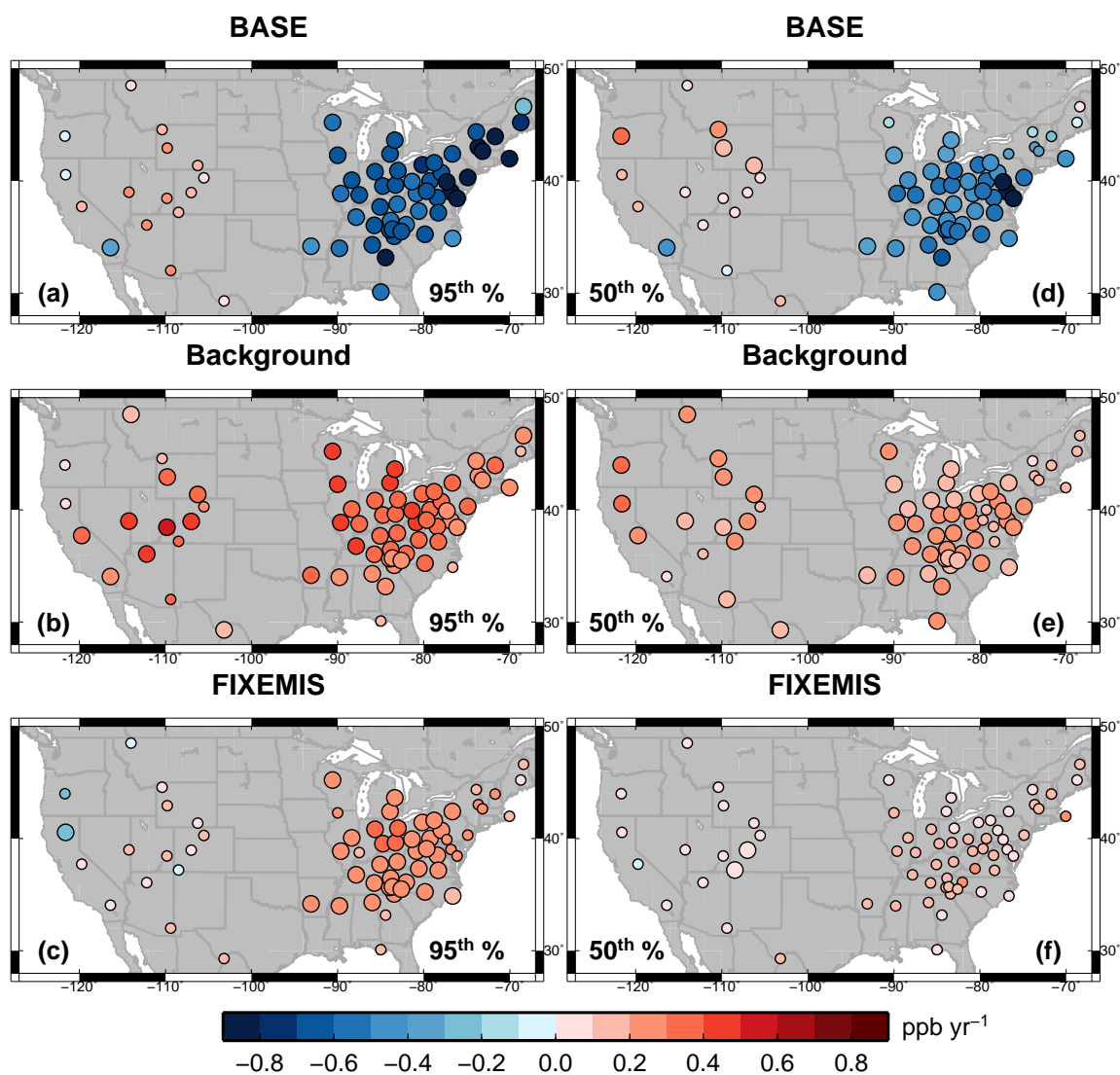
Figure 11. As in Figure 10, but for summer. Top panels are repeated from Fig. 8d,e.
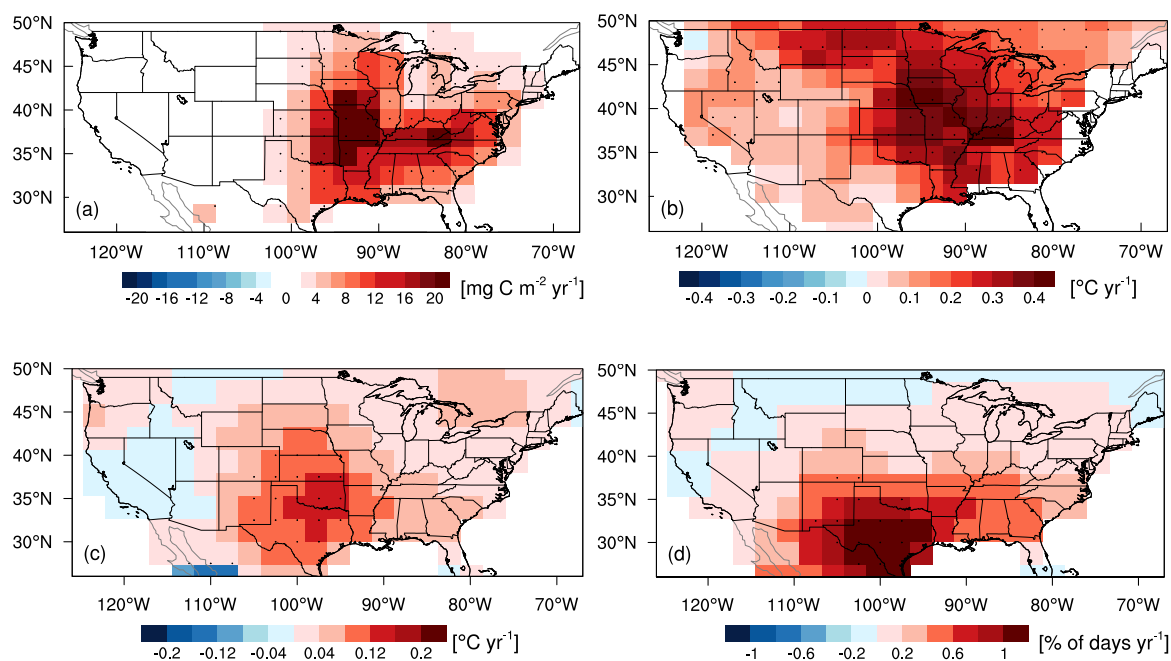
Figure 12. The 1990-2012 trends in: (a) model JJA total biogenic isoprene emissions; (b) model 90th percentile JJA daily maximum temperature; (c) the warmest daily maximum temperature and (d) the frequency of warm days (i.e., those above the 90th percentile for the base period 1961-90) for August obtained from GHCNDEX dataset (Donat et al., 2013; available at http://www.climdex.org/view_download.html). Stippling denotes areas where the change is statistically significant ($p<0.05$). Note that the trends are calculated for the 1990-2012 period, instead of 1988-2014, to avoid the influence from hot extremes in 1988 and cold conditions in 2014 (Sect. 6). When these years are included, the trends in (c) and (d) are swamped by the anomalies. The trends in (a) and (b) are similar between 1990-2012 and 1988-2014.

Atmospheric
Chemistry
and Physics
Discussions

Open Access

EGU
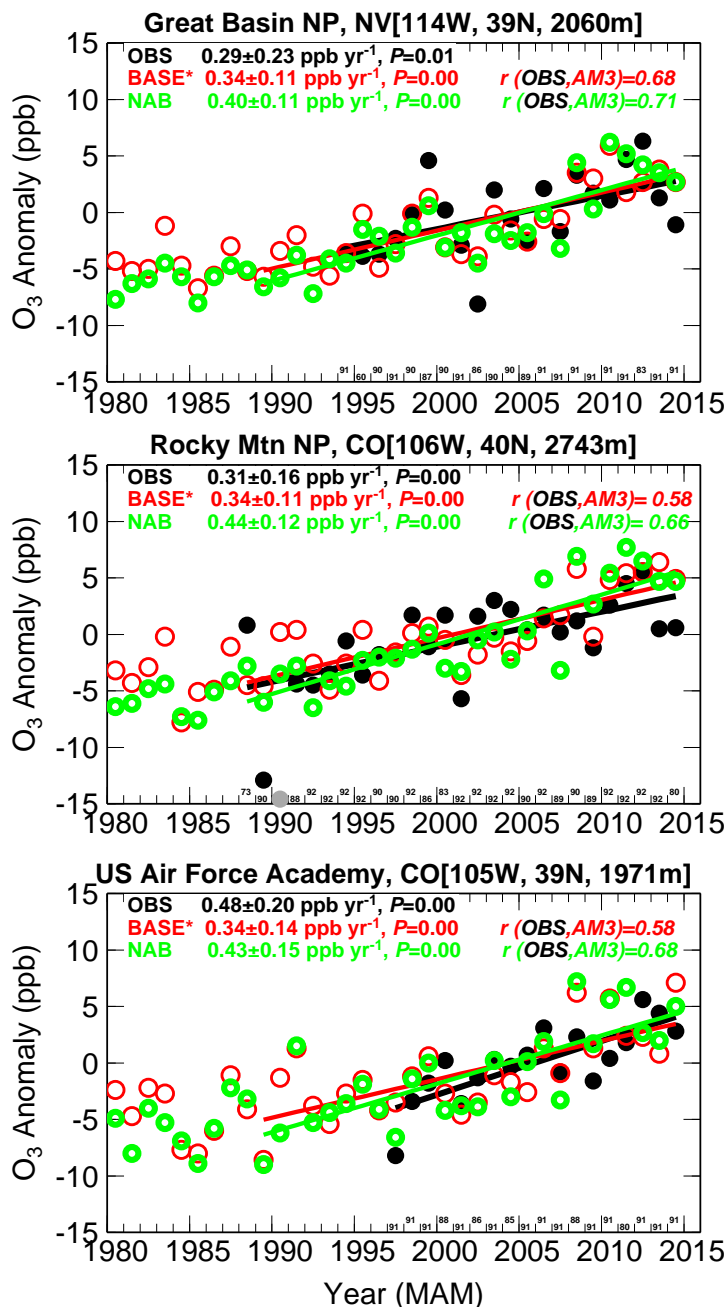
Figure 13a. Time series of median spring MDA8 O_3 anomalies (relative to the 1995-2014 mean) at Great Basin, Rocky Mountain, and US Air Force Academy as observed (black) and simulated in AM3_BASE filtered for baseline conditions (red, see Sect.2.4) and in Background with North American anthropogenic emissions zeroed out (NAB; green). Presented on the top of the graph are statistics from the linear fit and correlations between observations and simulations. Numbers on the bottom of the graph denote the sample size of observations for each year. Grey dots indicate uncertain observations that are removed from the linear fit (see Sect. 2.3).
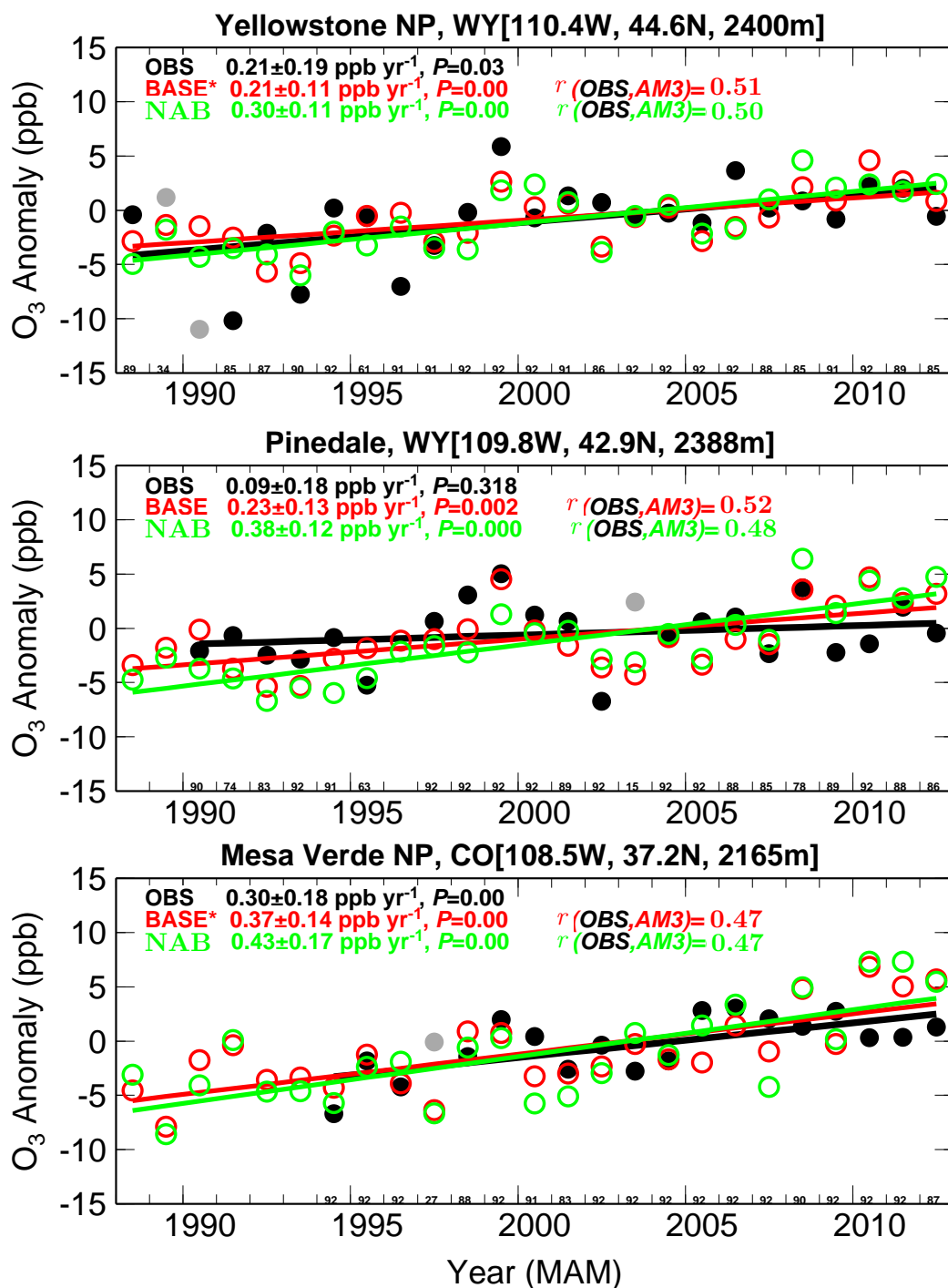
Figure 13b. Same as Figure 13a, but for Yellowstone, Pinedale, and Mesa Verde over the period 1988-2012.
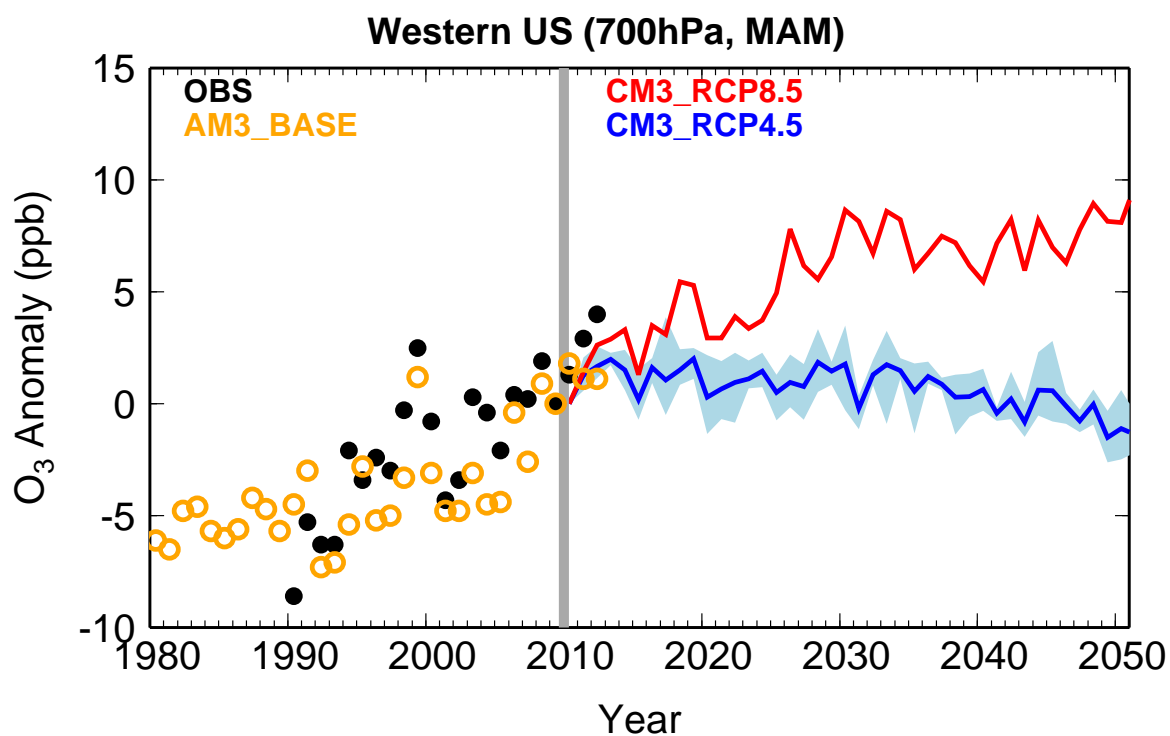
Figure 14. Future projections. Time series of median springtime O_3 changes relative to 2010 over the WUS (35-45N,120-105W) in GFDL AM3 hindcast (orange circles) and CM3 future simulations for RCP8.5 (red) and RCP4.5 (blue; shading represents the range of three ensemble members). Black circles indicate observed changes averaged from Lassen, Great Basin, and Rocky Mountain National Parks.
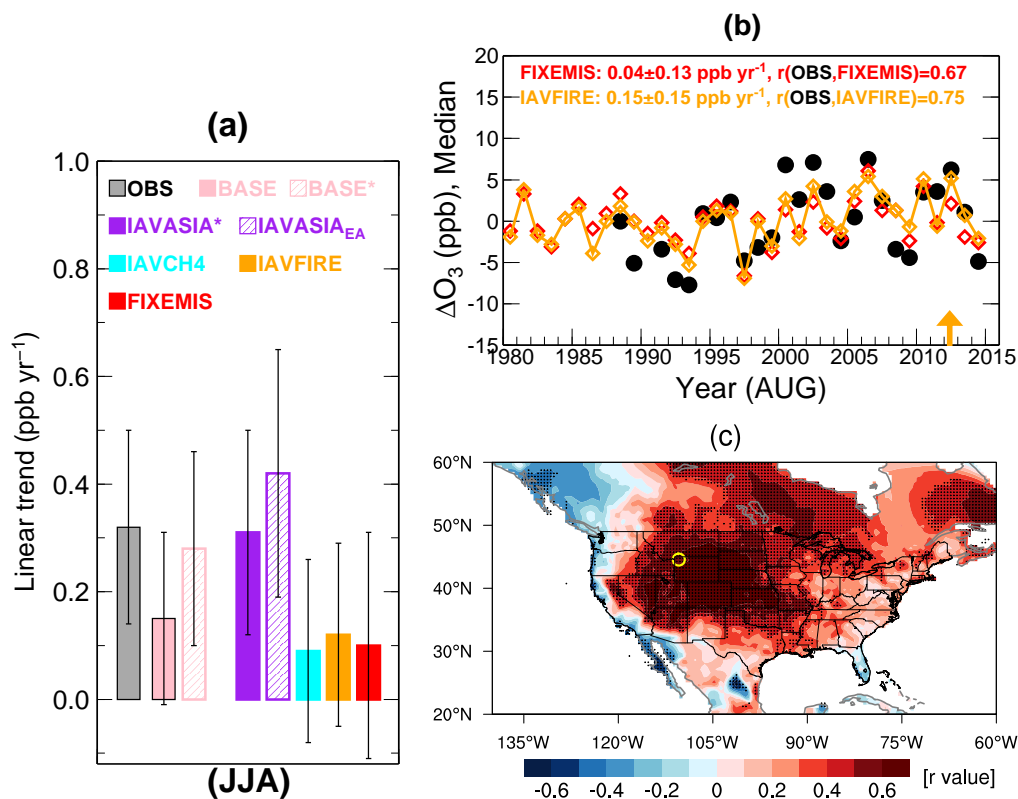
Figure 15. **Variability and trends of summertime O$_3$ at Yellowstone National Park.** (a) Median JJA MDA8 O$_3$ trends over 1988-2012 at Yellowstone from observations (black) and simulations sampled at 700 hPa for BASE without filtering (pink), BASE filtered for baseline conditions (hatched pink), IAVASIA (solid purple, baseline), IAVASIA filtered for Asian influence (EACOt≥67th, hatched purple), IAVCH$_4$ (cyan), IAVFIRE (orange) and FIXEMIS (red). (b) Time series of anomalies in August median MDA8 O$_3$ at Yellowstone as observed (black) and simulated by the model sampled at the surface, with constant (red) and time-varying wildfire emissions (orange). Trends in (b) are reported for the 1988-2014 period. (c) Interannual correlations of JJA mean MDA8 O$_3$ observed at Yellowstone with JJA mean daily maximum temperature from observations (Harris et al., 2014).
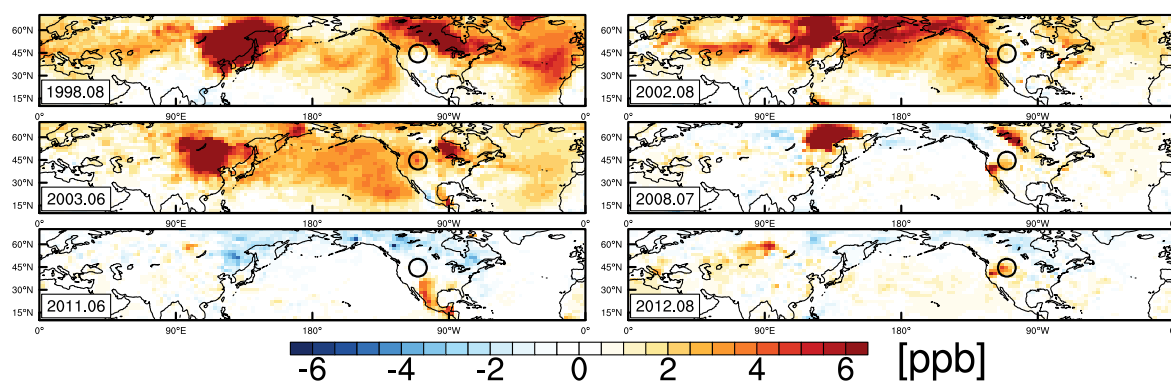
Figure 16. Surface MDA8 O_3 enhancements from wildfire emissions for individual months in the years with large biomass burning in boreal regions (1998, 2002, 2003) and over the WUS (2008, 2011, 2012), as diagnosed by the differences between IAVFIRE and FIXEMIS. The black circle denotes the location of Yellowstone National Park.
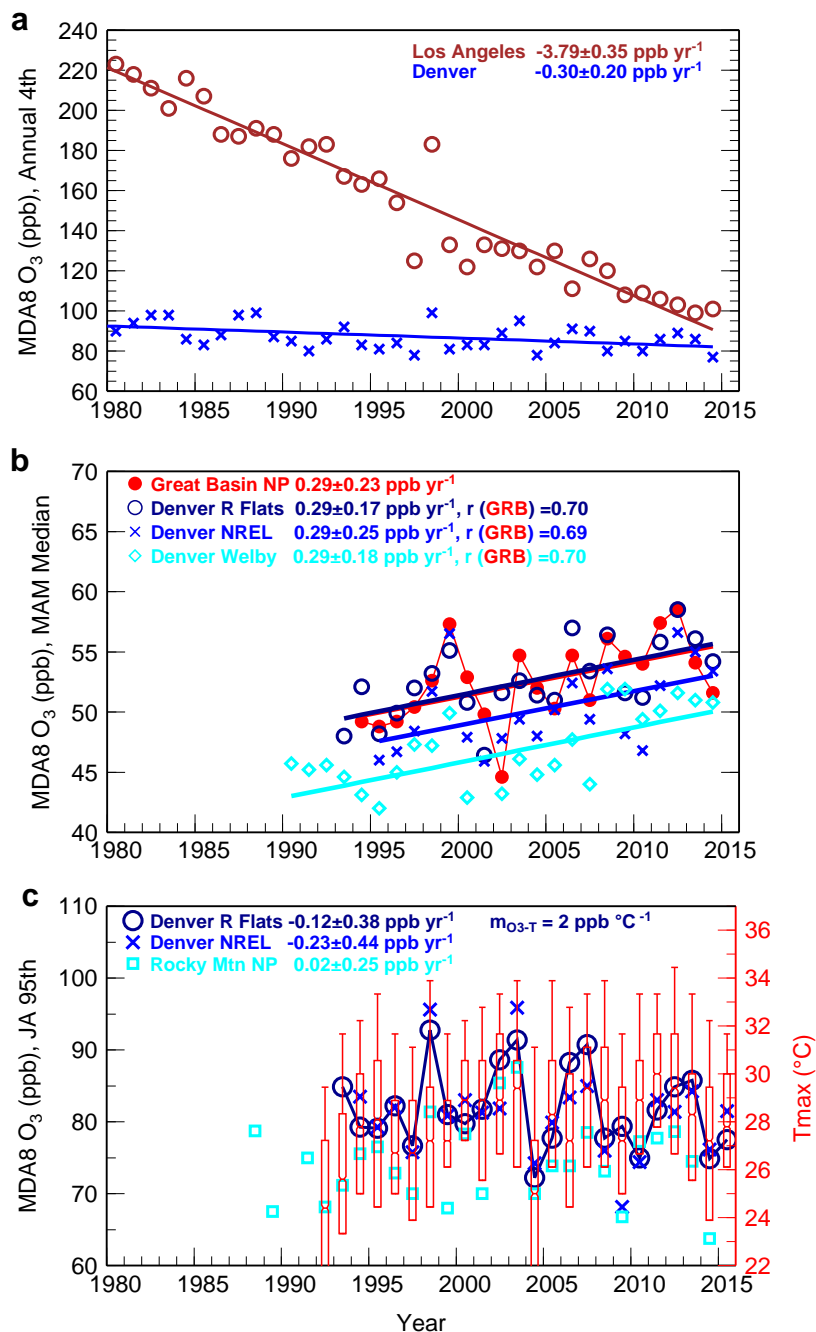
Figure 17. **Surface O$_3$ trends in Denver.** (a) Comparison of observed trends in annual 4th highest MDA8 O$_3$ at Crestline Los Angeles (brown) and in Denver (blue, computed from all monitors available in Denver non-attainment counties). (b) Time series of observed median MAM MDA8 O$_3$ at Great Basin National Park (red), in comparison with three monitors in Denver. (c) Time series of observed 95th percentile July-August MDA8 O$_3$ in Denver, together with statistics (25th, 50th, 75th, 95th) of observed July-August daily maximum temperature at Rocky Flats (red, right axis).

Atmospheric
Chemistry
and Physics
Discussions

Open Access
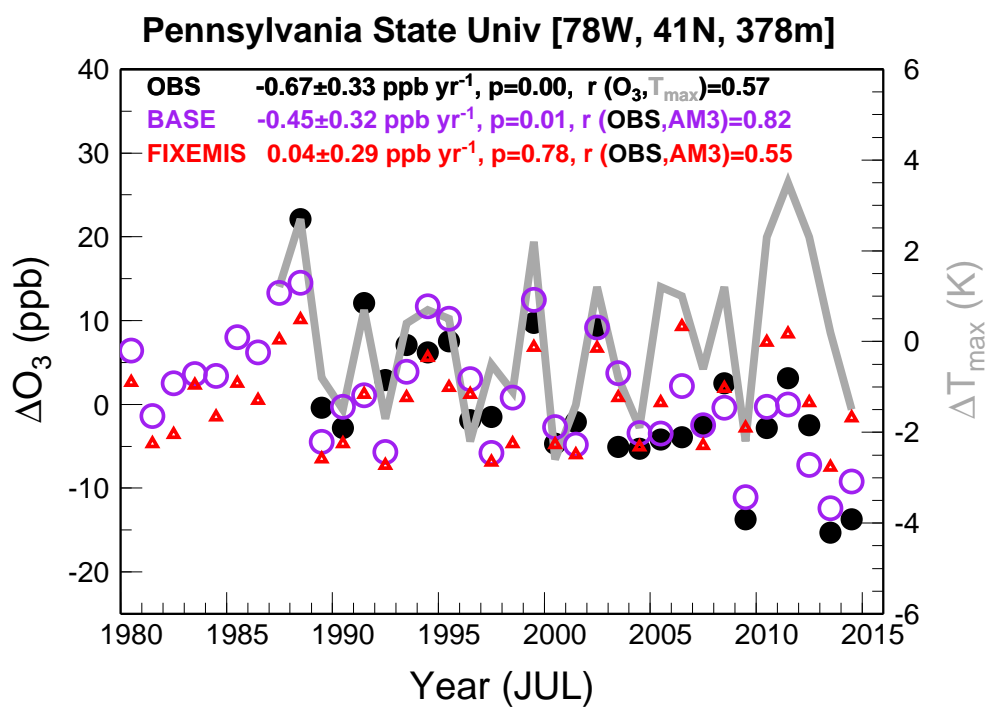
Figure 18. Anomalies in July mean MDA8 O_3 at the Pennsylvania State CASTNET site as observed (black) and simulated by the GFDL-AM3 model with time-varying (purple) and constant anthropogenic emissions (red). Observed anomalies in July mean daily maximum temperature are shown in gray using right axis.
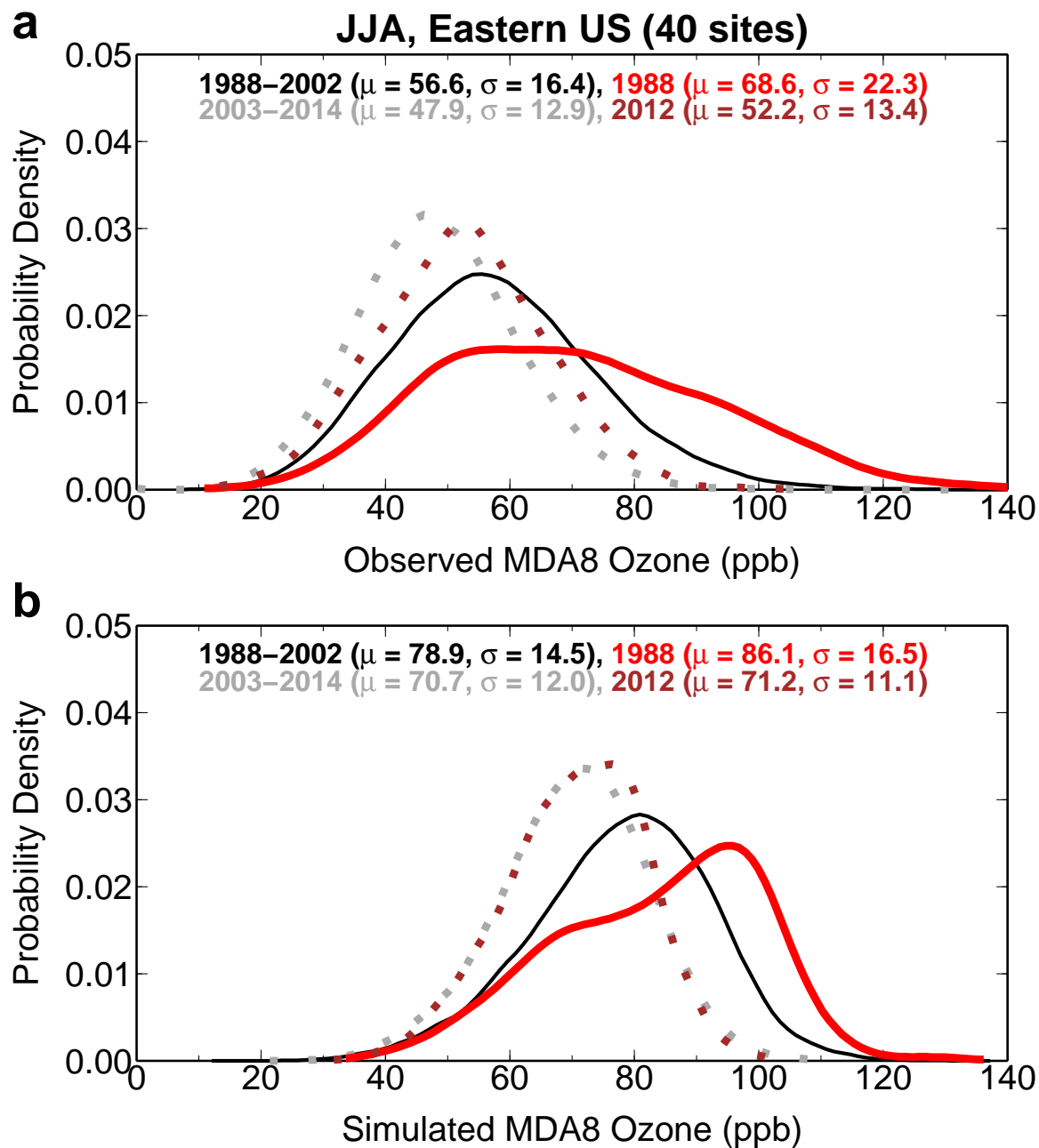
Figure 19. (a) Comparisons of probability distributions of summertime MDA8 O_3 from CASTNet over the EUS domain for the pre-NO_x SIP Call (1988-2002; solid black lines) versus post-NO_x SIP Call (2003-2014; dashed gray lines) periods and during the extreme heat waves of 1988 (solid red lines) versus 2012 (dashed brown lines). (b) Same as (a) but from AM3_BASE. The median (μ) and standard deviation (σ) are shown (ppb).
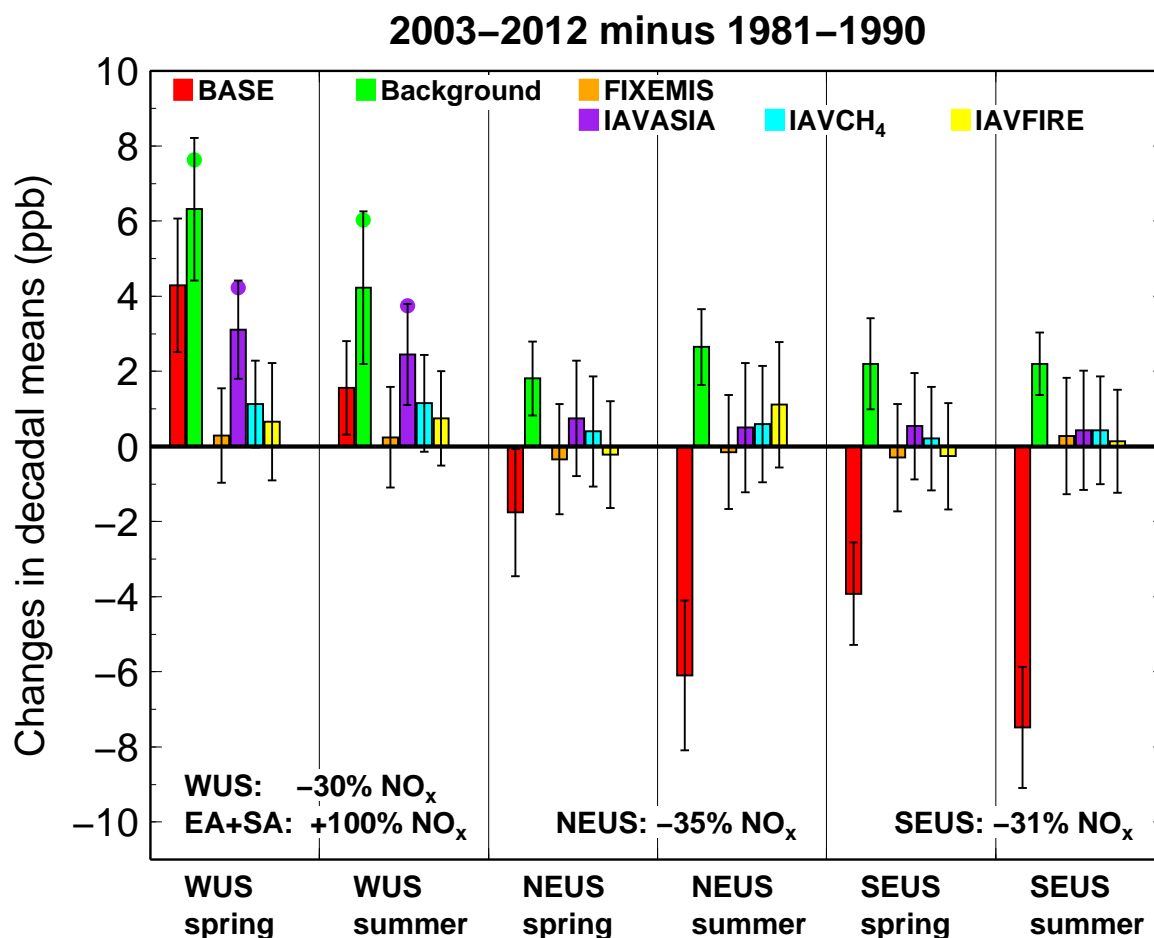
Figure 20. **Summary of US surface O$_3$ trends and drivers.** Changes in decadal mean MDA8 O$_3$ from 1981-1990 to 2003-2012 simulated in a suite of GFDL-AM3 experiments for spring and summer for the western (32N-46N and 123W-102W), Northeast (37N-45N and 90W-65W) and Southeast (30N-36N and 95W-77W) US domains. Experiments are color-coded with the error bars indicating the range of the mean change at the 95% confidence level. Filled circles represent the changes under Background (green) and IAVASIA (purple) when filtered for Asian influence (EACOt$\geq$67th%), while other results are from the unfiltered models. The text near the bottom of the plot provides the change in NO$_x$ emissions over the same period for each region.

Atmospheric
Chemistry
and Physics
Discussions

Table 1 Summary of forcings and emissions used in AM3 hindcasts and CM3 projections

Experiment	Time Periods	Meteorology	Radiative forcings	CH$_4$ (chemistry)	Anthropogenic emissions	Fire Emissions
BASE	1979-2014	Nudged to NCEP	Historical	Historical	Historical	Historical
Background	1979-2014	as BASE	Historical	Historical	Zeroed out in N. America; As BASE elsewhere	Historical
FIXEMIS	1979-2014	as BASE	Historical	2000	Constant*	Constant*
IAVFIRE	1979-2014	as BASE	Historical	2000	Constant*	Historical
IAVASIA	1979-2012[+]	as BASE	Historical	2000	Varying in Asia as BASE; as in FIXEMIS elsewhere	Constant*
IAVCH$_4$	1979-2012[+]	as BASE	Historical	Historical	Constant*	Constant*
CM3_RCP4.5	2005-2050	Free running	RCP4.5	RCP4.5	RCP4.5	RCP4.5
CM3_RCP8.5	2005-2050	Free running	RCP8.5	RCP8.5	RCP8.5	RCP8.5

*Averaged over the whole 1970-2010 period.

+Note that the IAVASIA and IAVCH$_4$ simulations only extend to 2012.

Atmospheric
Chemistry
and Physics
Discussions

Table 2. Summary of linear trends in spring MDA8 O_3 for 1988 to 2012 (ppb yr^{-1}) observed at seven western U.S. sites and as simulated in the AM3 experiments. Trends with the 95% confidence intervals and levels of significance (**bold**: <1%; *italic*, 1-5%; ▢, ≥5%) were estimated by the two-tailed *t*-test.

Experiment[a]	Lassen	Great Basin	Rocky Mountain	Mesa Verde	Yellowstone	Yosemite	Chiricahua
			Spring (MAM)				
Observed	**0.38±0.14**	**0.38±0.26**	**0.37±0.18**	**0.30±0.18**	*0.21±0.19*	*0.37±0.32*	**0.17±0.10**
BASE*	**0.33±0.11**	**0.34±0.12**	**0.32±0.13**	**0.37±0.14**	**0.21±0.11**	**0.35±0.17**	*0.25±0.19*
Background	**0.31±0.12**	**0.40±0.13**	**0.45±0.13**	**0.43±0.17**	**0.30±0.11**	**0.41±0.16**	**0.32±0.21**
Background$_{EA}$	**0.41±0.12**	**0.39±0.18**	**0.50±0.15**	**0.52±0.20**	**0.40±0.16**	**0.47±0.17**	**0.47±0.21**
IAVASIA*	**0.29±0.13**	**0.31±0.11**	**0.25±0.11**	**0.27±0.11**	**0.19±0.11**	**0.24±0.14**	0.15±0.15
IAVASIA$_{EA}$	**0.26±0.16**	**0.26±0.16**	**0.35±0.13**	**0.32±0.13**	**0.27±0.16**	**0.31±0.18**	**0.25±0.15**
IAVCH$_4$*	*0.18±0.12*	**0.20±0.11**	*0.12±0.09*	*0.16±0.12*	0.09±0.12	0.15±0.16	0.04±0.15
IAVFIRE	0.10±0.12	*0.14±0.12*	*0.17±0.14*	*0.16±0.14*	0.11±0.13	0.15±0.16	0.08±0.17
FIXEMIS	0.08±0.12	*0.12±0.12*	*0.16±0.12*	*0.13±0.12*	0.09±0.13	0.12±0.16	0.04±0.16
O$_3$Strat	0.18±0.18	0.20±0.25	0.18±0.18	*0.25±0.23*	0.15±0.18	0.27±0.30	0.07±0.24

a. The * mask indicates data filtered to represent baseline conditions (NACOt ≤67th). The EA subscript indicates that data were filtered to represent transport conditions favoring the import of Asian pollution (EACOt ≥ 67th).